

## Journal Pre-proof

Optimization of Triple-Pressure Combined-Cycle Power Plants by Generalized Disjunctive Programming and Extrinsic Functions

Juan I. Manassaldi , Miguel C. Mussati , Nicolás J. Scenna , Sergio F. Mussati

PII: S0098-1354(20)31233-3  
DOI: <https://doi.org/10.1016/j.compchemeng.2020.107190>  
Reference: CACE 107190



To appear in: *Computers and Chemical Engineering*

Received date: 20 August 2020  
Revised date: 13 October 2020  
Accepted date: 30 November 2020

Please cite this article as: Juan I. Manassaldi , Miguel C. Mussati , Nicolás J. Scenna , Sergio F. Mussati , Optimization of Triple-Pressure Combined-Cycle Power Plants by Generalized Disjunctive Programming and Extrinsic Functions, *Computers and Chemical Engineering* (2020), doi: <https://doi.org/10.1016/j.compchemeng.2020.107190>

This is a PDF file of an article that has undergone enhancements after acceptance, such as the addition of a cover page and metadata, and formatting for readability, but it is not yet the definitive version of record. This version will undergo additional copyediting, typesetting and review before it is published in its final form, but we are providing this version to give early visibility of the article. Please note that, during the production process, errors may be discovered which could affect the content, and all legal disclaimers that apply to the journal pertain.

© 2020 Published by Elsevier Ltd.

# Optimization of Triple-Pressure Combined-Cycle Power Plants by Generalized Disjunctive Programming and Extrinsic Functions.

Juan I. Manassaldi<sup>a</sup>, [jmanassaldi@frro.utn.edu.ar](mailto:jmanassaldi@frro.utn.edu.ar), Miguel C. Mussati<sup>a,b</sup>, [mmussati@santafe-conicet.gov.ar](mailto:mmussati@santafe-conicet.gov.ar),

Nicolás J. Scenna<sup>a</sup>, [nscenna@santafe-conicet.gov.ar](mailto:nscenna@santafe-conicet.gov.ar), Sergio F. Mussati<sup>a,b,\*</sup>, [mussati@santafe-conicet.gov.ar](mailto:mussati@santafe-conicet.gov.ar)

<sup>a</sup>CAIMI, UTN FRRO, Zeballos 1341, S2000BQA, Rosario, Argentina, Tel.: +54 341 4480102,

<sup>b</sup>INGAR (CONICET-UTN) - Instituto de Desarrollo y Diseño, Avellaneda 3657, 3000, Santa Fe, Argentina

\*Corresponding author

## Highlights

- Dynamic-link libraries implemented in the C programming **language**.
- Successful application of extrinsic functions and GDP model to optimize CCPPs.
- Improved optimal solutions with respect to reference cases.

## Abstract

A new mathematical framework for optimal synthesis, design, and operation of triple-pressure steam-reheat combined-cycle power plants (CCPP) is presented. A superstructure-based representation of the process, which embeds a large number of candidate configurations, is first proposed. Then, a generalized disjunctive programming (GDP) mathematical model is derived from it. Series, parallel, and combined series-parallel arrangements of heat exchangers are simultaneously embedded. Extrinsic functions executed outside GAMS from dynamic-link libraries (DLL) are used to estimate the thermodynamic properties of the working fluids. As a main result, improved process configurations with respect to two reported reference cases were found. The total heat transfer areas calculated in this work are by around 15% and 26% lower than those corresponding to the reference cases.

This paper contributes to the literature in two ways: (i) with a disjunctive optimization model of natural gas CCPP and the corresponding solution strategy, and (ii) with improved HRSG configurations.

## Keywords

Generalized Disjunctive Programming; Extrinsic Functions; Three-Pressure Reheat Combined-Cycle Power Plant; Heat Recovery Steam Generator HRSG; GAMS

34

35

36 **Notation**37 **Sets**

38 HE( $i,j,k$ ) contains the heat exchangers located in the section  $i$  and pressure level  $j$  with the stream  
39  $k$

40 EV( $i$ ) contains the sections where the evaporators are located.

41 PUMP( $n,k,k'$ ) contains the pump number  $n$  with the corresponding inlet stream  $k$  and outlet stream  $k'$

42 NHNP( $i,j,n$ ) contains the economizers located in the section  $i$  and pressure level  $j$  associated to the  
43 pump  $n$

44 HNP( $i,j,n$ ) contains the heat exchangers located in the section  $i$  and pressure level  $j$  associated to  
45 the pump  $n$

46 **Indices**

47  $i$  sections of the heat recovery steam generator

48  $j$  pressure levels in the heat recovery steam generator

49  $k$  water stream number

50  $n$  pump number

51 **Positive Variables**

52  $A_{\text{COND}}$  Heat transfer area of the condenser in the Rankine cycle ( $\text{m}^2$ )

53  $A_{i,j}$  Heat transfer area of corresponding to the heat exchanger located in the section  $i$  and pressure  
54 level  $j$  ( $\text{m}^2$ )

55  $h_i^G$  Enthalpy of the flue gas stream  $G$  in the section  $i$  ( $\text{kJ kg}^{-1}$ )

56  $h_k$  enthalpy of the stream  $k$  ( $\text{kJ kg}^{-1}$ )

57  $m_k$  mass flowrate of the stream  $k$  ( $\text{kg s}^{-1}$ )

58  $m^G$  mass flowrate of the flue gas stream  $G$  ( $\text{kg s}^{-1}$ )

59  $Q_{i,j}$  heat load in the heat exchanger located in the section  $i$  and pressure level  $j$  (MW)

60  $\Delta T_{i,j}$  driving force corresponding to the heat exchanger located in the section  $i$  and pressure level  $j$   
61 (K)

62  $T_i^G$  temperature of the fluegas steam  $G$  in the section  $i$  (K)

63  $T_k$  temperature of the stream  $k$  (K)

64  $W$  net electrical power (MW)

65  $\Delta T_{i,j}$  driving force corresponding to the heat exchanger located in the section  $i$  and pressure level  $j$   
 66 (K)

67 **Variables**

68 THTA total heat transfer area ( $\text{m}^2$ )

69 **Binary variables**

70  $x_{i,j}$  existence of the heat exchanger in the section  $i$  and pressure level  $j$

71  $y_n$  existence of the pump  $n$

72  $z_k$  existence of the stream  $k$  associated to reheating

73 **Parameter**

74  $EC_j$  maximum number of economizers operating in the pressure level  $j$

75  $PE_i$  maximum number of heat exchangers operating in parallel at the section  $i$

76  $SH_j$  maximum number of superheaters operating in the pressure level  $j$

77  $U_{i,j}$  overall heat transfer coefficient ( $\text{W m}^{-2} \text{K}^{-1}$ )

78 **Acronyms**

79 BARON branch-and-reduce optimization navigator

80 CCPPs combined-cycle power plants

81 CHP combined heat and power

82 DLL dynamic-link library

83 GA genetic algorithms

84 GAMS general algebraic modeling system

85 GDP generalized disjunctive programming

86 HP high pressure

87 HRSGs heat recovery steam generators

88 IGCC integrated gasification combined cycle

89 LP low pressure

90 MINLP mixed-integer nonlinear programming

91 MP medium pressure

92 NGCC natural gas combined cycle power plants

93 NLP nonlinear programming

94 ORC organic Rankine cycles

95 PUMP pump

96 SA simulated annealing

97 SBB standard branch and bound

98 ST1 steam turbine 1

99 ST2 steam turbine 2

100 ST3 steam turbine 3

101

102

103

## 104 1. Introduction

105 Combined cycle power plants (CCPP) are widely used industrial plants or larger distribution  
106 networks to provide both electricity and heat as energy vectors. The overall thermal efficiency of  
107 combined-cycle power plants (CCPPs) depends strongly on the gas and steam turbine technologies as  
108 well as the configuration and design of the heat recovery steam generators (HRSGs). Improved CCPPs  
109 lead to reduce fuel consumption and, consequently, the greenhouse gas emissions. The configuration,  
110 design, and operating conditions of HRSGs are critical because they couple the gas turbine-based  
111 topping cycle with the steam turbine-based bottoming cycle. The exhaust waste energy of gas turbines  
112 can be recovered in HRSGs using different reheat cycles: from a single-pressure to triple-pressure  
113 cycles. In a CCPP, the optimal configuration of the HRSG depends strongly on the desired level of  
114 electricity to be generated, and, if it is the case, on the amount of steam required as utility heating if the  
115 CCPP is integrated to an industrial plant. Therefore, it is of great interest to still study the optimization  
116 of CCPPs through detailed process models and simultaneous optimization methods (Blumberg et al.,  
117 2017; Nadir and Ghenaiet, 2015), as it is proposed in this paper.

118 There are many published papers addressing the mathematical modeling and optimization of  
119 combined heat and power (CHP) generation systems, which differ in the criteria used to solve the  
120 resulting mathematical models (energy, exergy, cost, exergo-economic analyses, simulation-based  
121 optimization, simultaneous optimization, or meta-heuristic approaches), the number of optimization  
122 criteria (single or multi-objective optimization), and/or the model assumptions and design  
123 specifications considered for the analysis (fixed or variable process configurations, fixed or variable  
124 number of pressure levels, fixed or variable amount of steam and/or electricity to be generated).

125 Exergy and exergo-economic analyses of energy conversion systems to systematically locate the  
126 most inefficient system components have been used as a valuable decision-making tool (Bracco and  
127 Siri, 2010; Boyaghchi and Molaie, 2015; Bakhshmand et al., 2015; Tsatsaronis and Park, 2002;  
128 Morosuk and Tsatsaronis, 2011; Tsatsaronis, 1999; Sahoo, 2008; Ahmadi and Dincer, 2011). For  
129 instance, the retrofit of an already existing process can be improved by switching out and/or  
130 introducing new components towards a lower value of the total irreversibility of the system. These

131 analyses are iterative in nature and contribute to improving a thermal system as a whole or at a  
132 component level. Although the calculation of exergy is more complex than the calculation of energy,  
133 the exergy analysis allows quantifying more accurately the types, causes, and locations of  
134 inefficiencies. Bakhshmand et al. (2015) performed an exergo-economic analysis and optimization of a  
135 triple-pressure combined cycle. To do this, they implemented a simulation code in MATLAB using an  
136 evolutionary algorithm. The objective function included both product cost rate and cost rates  
137 associated with exergy destruction. The obtained results allowed to propose optimal performance  
138 criteria for the studied process. The authors highlighted that this methodology is applicable to optimize  
139 steady state operation parameters of a given combined cycle, but it is not suitable to optimize the  
140 design of new cycles. Tsatsaronis and Park (2002) and Morosuk and Tsatsaronis (2011) concluded  
141 about the advantages of dividing exergy destruction and economic costs into avoidable and  
142 unavoidable parts in cogeneration plants (Tsatsaronis and Park, 2002) and simple gas turbine systems  
143 (Morosuk and Tsatsaronis, 2011), showing the potential for improvement and the interactions among  
144 the system components. In exergy analyses, structural coefficients are used to consider how the overall  
145 irreversibility of the cycle is influenced by the local irreversibilities of each component. These  
146 structural coefficients can be calculated once the irreversibilities of the components and the whole  
147 cycle are known. Therefore, in a system with many components with a large number of discrete  
148 decisions, the calculation of these coefficients may require a high number of simulation runs resulting  
149 in a time-consuming procedure (Tsatsaronis, 1999). Most exergy and exergo-economic optimization  
150 approaches are subjective in nature as they require the designer's interpretation at each iteration to find  
151 the final configuration (Sahoo, 2008).

152 On the other hand, the degree of development of the optimization methods and software, and  
153 the availability of powerful computational systems have motivated a renewed interest in applying  
154 evolutionary algorithms, mathematical programming techniques in industry, including utility plants  
155 and CHP systems.

156 Applications of evolutionary algorithms – such as simulated annealing (SA) and genetic  
157 algorithms (GA) – can be found in Ahmadi and Dincer, 2011; Ahmadi et al., 2012; Kaviri et al., 2012;  
158 Mehrpanahi et al., 2019; Ameri et al., 2018; Mehrgoo et al., 2017; Naserabad et al., 2018; Rezaie et al.,  
159 2019). These algorithms have been successfully applied for optimization of power plants with known  
160 (fixed) configurations. GAs and derivative-free algorithms are well suitable when no information is  
161 available about the gradient of the function at the evaluated points. As GAs can be parallelized with  
162 little effort, a lot of paths to the optimum are considered in parallel, which is important in high-  
163 complexity problems with many solutions. However, GAs require many parameters, such as the

164 number of generations, population, crossover and mutation rates, and tournament size (number of  
165 individuals needed to fill a tournament during selection) that can significantly affect the obtained  
166 solutions.

167 The use of advanced optimization methods and the development of rigorous mathematical  
168 models made possible to find new HRSG configurations with the corresponding optimal operating  
169 conditions. In this context, there are several articles addressing the study of energy systems, including  
170 power and heat plants, which employ [gradient-based](#) optimization algorithms and deterministic mixed-  
171 integer nonlinear programming techniques (MINLP). The use of MINLP techniques for some  
172 representative applications can be found in Kim and Edgar (2014) and particularly in Gopalakrishnan  
173 and Kosanovic (2015) for optimal scheduling of CHP plants, in Santos and Urtubey (2018) for optimal  
174 energy dispatch in cogeneration plants, in Elsidio et al. (2017) for optimal design of organic Rankine  
175 cycles (ORC), and in Perez-Uresti et al. (2019) for optimal design of renewable-based utility plants.  
176 Other applications include the design of supercritical coal-fired power plants (Wang et al., 2014),  
177 short-term planning of cogeneration power plants (Taccari et al., 2015; Bruno et al., 1998), optimal  
178 synthesis and design of single and/or dual-purpose seawater desalination plants (Tanvir and Mujtaba,  
179 2008; Mussati et al., 2003a; Mussati et al., 2003b; Mussati et al., 2004; Mussati et al., 2005), as well as  
180 optimal integration of natural gas combined cycle (NGCC) power plants and CO<sub>2</sub> capture plants  
181 (Manassaldi et al., 2014; Mores et al., 2018). Also, MINLP models were successfully applied in other  
182 areas such as design of water and wastewater treatment processes (Lu et al., 2017; Faria and  
183 Bagajewicz, 2012; Ahmetovic and Grossmann, 2011), heat exchanger network in fuel processing  
184 systems for PEM fuel cells (Oliva et al., 2011), design and dispatch of SOFC-based CCHP system  
185 (Jing et al., (2017), scheduling and retrofit of refinery preheat trains (Izyan et al., 2014), among other  
186 applications. [Leon and Martin \(2016\)](#) addressed the optimization of a combined cycle power plant by  
187 [considering biogas as fuel](#). To this end, the authors implemented a mixed integer nonlinear  
188 [programming \(MINLP\) model in GAMS](#) and investigated two alternative schemes for the steam  
189 [production](#). The calculation of the thermodynamics for the steam was included in the model via  
190 [surrogate models](#). Although MINLP formulations are in general hard to solve (especially when the  
191 feasible regions are non-convex), they are the most suitable alternative for highly nonlinear and  
192 combinatorial optimization problems and large-size mathematical models (problems involving many  
193 discrete and continuous decisions and nonlinear equality constraints). In this work, due to the  
194 characteristics of the proposed optimization models, the MINLP technique is used.

195 Despite the existence of many articles concerning with the study of NGCC power plants under  
196 different assumptions and using different computational tools, only a few papers considering the

197 simultaneous optimization of the HRSG configuration, process-unit sizes, and operating conditions can  
198 be found in literature (Ahadi-Oskui et al., 2010, Martelli et al., 2017; Zhang et al., 2014; Manassaldi et  
199 al., 2016; Franco and Giannini, 2006). Ahadi-Oskui et al. (2010) applied mathematical programming  
200 methods to simultaneously optimize the configuration and operating conditions of a combined-cycle-  
201 based cogeneration plant. To this end, the authors formulated a nonconvex mixed-integer nonlinear  
202 problem (MINLP). The resulting model was successfully solved by using their own MINLP solver  
203 called LaGO which generates a convex relaxation of the MINLP and applies a Branch and Cut  
204 algorithm to the relaxation. Martelli et al. (2017) proposed a two-stage methodology to optimize  
205 HRSGs of simple CHP cycles considering external heat/steam sources/users with the possibility of  
206 multiple supplementary firing. The proposed methodology was clearly described through an integrated  
207 gasification combined cycle (IGCC) plant with CO<sub>2</sub> capture. Zhang et al. (2014) proposed a  
208 superstructure-based MINLP model to optimize the configuration of a HRSG embedding several  
209 candidate matches between the HRSG and external heat flows. The resulting model is non-convex  
210 because of the presence of bilinear terms. The solver BARON (Branch-And-Reduce Optimization  
211 Navigator) (Sahinidis, 2000), which is supported in GAMS (General Algebraic Modeling System)  
212 (Brooke et al., 1992), was used as a global optimizer. Several case studies considering different  
213 pressure levels, with and without steam reheating, were successfully solved. Franco and Giannini  
214 (2006) proposed a two-level optimization framework of HRSGs. The former level consists on  
215 obtaining the main operating conditions, and the second one the detailed design of each section (sizes  
216 and geometric variables). The framework uses the optimal output of the first level as the input to the  
217 second level. The authors successfully verified the proposed framework using already existing HRSG  
218 structures. Also, simultaneous optimization has been successfully applied to other integrated systems  
219 such as biomass Fischer-Tropsch liquids plants. Manassaldi et al. (2016) proposed a discrete and  
220 continuous mathematical model to optimize the synthesis and design of dual-pressure HRSGs coupled  
221 to two steam turbines. The optimization problem consisted in determining how the heat exchangers  
222 (economizers, evaporators, and superheaters) should be connected in the HRSG to maximize the total  
223 net power keeping fixed the total heat transfer area, or either to minimize the total heat transfer area  
224 keeping fixed the total net power. Also, the optimal operating conditions and size of each process unit  
225 were determined simultaneously. The resulting MINLP problem was solved using SBB (Standard  
226 Branch and Bound) (Bussieck and Drud, 2001) and the solver CONOPT for the nonlinear problems  
227 (NLP) (Drud, 1992). The authors found a novel HRSG configuration not previously reported in the  
228 literature. Recently, Bongartz et al. (2020) discussed three bottoming cycles for combined cycle power  
229 plants of increasing complexity. The authors employed their open-source deterministic global solver



230 MAiNGO and developed a novel method for constructing relaxations of the functions reported in  
231 IAPWS-IF97 to calculate the thermodynamic properties of water and steam. The relaxations were  
232 implemented in the MC++ library (<https://omega-icl.github.io/mcpp/index.html>). The authors  
233 concluded that the proposed relaxations considerably reduce the computational time required to find  
234 the global optimal solution with respect to McCormick relaxations.

235 Generalized disjunctive programming (GDP) is an alternative modeling framework to represent  
236 optimization problems with discrete and continuous decisions (Chen and Grossmann, 2019). In GDP  
237 formulations, discrete decisions are represented in a natural way through the use of disjunctions in the  
238 continuous space and logic propositions in the discrete space which are then relaxed, obtaining a  
239 MINLP problem (Lee and Grossmann, 2000). GDPs can be reformulated via the convex hull  
240 (Grossmann and Lee, 2003) or via Big-M formulations (Grossmann and Ruiz, 2012). Vecchietti et al.  
241 (2003) developed the computer code LogMIP to solve discrete/continuous nonlinear optimization  
242 problems that are modeled with either algebraic, disjunctive, or hybrid formulations.

243 This paper is a natural continuation of the work presented by Manassaldi et al. (2016). Here,  
244 the superstructure-based model developed by Manassaldi et al. (2016) is used as a basis and it is  
245 properly extended to include three pressure levels as well as more candidate process configurations,  
246 thus highly increasing the combinatorial nature of the resulting superstructure-based optimization  
247 model. From a qualitative point of view, the main differences between this work and that of  
248 Manassaldi et al. (2016) are: (a) the type of the combined cycle to be studied (the inclusion of a third  
249 pressure level significantly increases the degrees of freedom for the optimization problems), (b) the  
250 mathematical modeling strategy (a generalized disjunctive programming (GDP) model is formulated  
251 instead of a pure MINLP model), and (c) the solution strategy includes a dynamic-link library (DLL)  
252 to estimate the thermodynamic properties of both circulating fluids (flue gas and water) at different  
253 conditions (in the case of water as subcooled and saturated liquid, saturated and superheated steam).  
254 On the other hand, the main difference between this work and papers published by other authors is the  
255 obtaining of improved configurations for a triple-pressure HRSG. Thus, to the best of our knowledge,  
256 this paper contributes to the literature of this field in two ways: (i) with a mathematical optimization  
257 model of NGCC power plants operated at three pressure levels and the corresponding solution  
258 strategy, and (ii) with improved HRSG configurations with respect to reference configurations taken  
259 from the literature.

260 The paper is organized as follows. Section 2 describes the process superstructure  
261 representation. Section 3 defines the problem statement. Section 4 presents the mathematical model.

262 Section 5 discusses the obtained results. Finally, Section 6 provides the conclusions of the  
263 investigation.

## 265 2. Process superstructure representation

266 As mentioned earlier, the heat exchangers in a HRSG operating at three pressure levels can be  
267 arranged in different ways. Also, the inlet of the working fluid in the HRSG can be located in the low-  
268 pressure (LP) level, or in the LP and medium-pressure (MP) levels, or in the LP, MP and high (HP)  
269 pressure levels. As an illustration, Fig. 1 presents three candidate configurations, which differ in the  
270 way of feeding the working fluid to the different pressure levels and in the location of some heat  
271 exchangers. It is important to mention here that there are many more ways to combine the heat  
272 exchangers, which are not shown in Fig. 1 but included in the formulation of the model.

273 In the process configuration shown in Fig. 1a, the three pressure levels are fed from the  
274 condenser. An LP economizer (section 10), an LP evaporator (section 9), and an LP superheater  
275 (section 8) are located in the coldest zone of the HRSG. Subsequently, in the intermediate-temperature  
276 zone, an MP economizer (section 7) and an MP evaporator (section 6) are located, followed by an HP  
277 economizer (section 5). Finally, in the hottest zone, an MP superheater, an HP evaporator, and a  
278 second MP superheater are placed, followed by an HP superheater (sections 4, 3, 2, and 1,  
279 respectively). In the process configuration shown in Fig. 1b, the LP and MP levels are fed from the  
280 condenser while the HP level is fed from the MP level. In this way, the HP economizer (section 5) is  
281 fed with a liquid stream with a temperature higher than that in Fig. 1a coming from the condenser, but  
282 implying a higher heat load in the MP economizer (section 8). On the other hand, the LP superheater –  
283 which was located in the section 8 in Fig. 1a – is now located in the section 7, where the gases can  
284 reach a higher temperature. Finally, in the process configuration shown in Fig. 1c, the MP and HP  
285 levels are fed from the corresponding inferior pressure level, i.e. the MP level from the LP level and  
286 the HP level from the MP level. This increases the temperature at which water enters the economizers  
287 but increases the heat load in the LP and MP levels (sections 9 and 7, respectively). **Also, unlike in the**  
288 **previous two cases, an MP superheater is removed and only one heat exchanger is kept in the hottest**  
289 **gas section (section 1).** In this configuration, the superheated steam stream coming from the steam  
290 turbines mixes with saturated steam and enters the unit of the section 1. In addition, the LP superheater  
291 is located in a zone hotter than in the previous configuration (Fig. 1b); indeed, it moves from the  
292 section 7 to 5.

293 In order to find the optimal configuration of the HRSG, the superstructure shown in Fig. 2 is  
294 proposed for optimization. As mentioned, this superstructure embeds, not only the process

295 configurations shown in Fig. 1, but also many other candidate configurations, where the heat  
296 exchangers are combined in different alternative arrangements (as will be detailed in the presentation  
297 of the mathematical model).

### 300 3. Optimization problem statement

301 Given are the process superstructure representation shown in Fig. 2 and the flow rate and inlet  
302 temperature of the flue gas stream. The optimization problem is formulated as follows.

303  
304  
305 Minimize (THTA)

306 subject to:

- 307 -Mass balances
- 308 -Energy balances
- 309 -Design equations (sizing)
- 310 -Thermodynamic property estimation equations
- 311 - Process design specifications (a fixed net electrical power generation).

312  
313 As result, the optimal values of the following decisions are obtained:

314 - Discrete decisions:

315 - Optimal structure (layout) of heat exchangers. This implies to select the number of the  
316 heat exchangers and their locations inside the HRSG indicating how they should be interconnected  
317 (series or series-parallel, or parallel arrangements).

318 - Optimal number of pressure levels. The results should indicate if the HRSG should be  
319 operated with three or two or one pressure levels. For instance, if the high pressure level is removed,  
320 the associated economizer, evaporator and superheater must be also removed.

321 - Optimal location of the reheating stream.

322 - Continuous decisions

323 - Optimal allocation of the total heat transfer area.

324 - Optimal values of mass flow rate, pressure, temperature, and composition of the process  
325 streams.

326 - Optimal heat loads at the system components.

328 The proposed optimization problem is solved and compared with two reference cases taken  
 329 from the literature. As will be shown in the next section, the main difference between the  
 330 superstructure here proposed and the configurations of the reference cases is the possibility of using  
 331 candidate pumps properly located to increase, if it is beneficial, the inlet pressure in the economizers.  
 332 Another difference is the consideration of more candidate configurations of heat exchangers as well as  
 333 different ways for steam reheating.

#### 335 4. Mathematical model

336 The entire mathematical model consists of the mass and energy balances of each process unit  
 337 (steam turbines, pumps, heat recovery steam generator), equations to calculate the associated heat  
 338 transfer areas, installed power of turbines and pumps, and equations to estimate the physico-chemical  
 339 properties of process streams. The main discrete decisions are those related to the configuration of the  
 340 heat exchangers in the HRSG and the selection of the corresponding pumps. The configuration of the  
 341 steam turbines is fixed but not their operating conditions and sizes. The main continuous decisions are  
 342 the pressure, temperature, and flow rate of the process streams of each working fluid (gas in the gas  
 343 turbine and water/steam in the steam turbines). Next, the main constraints used to model the discrete  
 344 decisions associated with the HRSG are presented.

##### 346 4.1 HRSG mathematical model

347 In order to perform an easier implementation of the model in GAMS and identification of each  
 348 heat exchanger, the HRSG is divided into several sections and pressure levels, as shown in Fig. 3. To  
 349 do this, the following sets are declared: the set 'I', with 13 elements 'i', is used to identify different  
 350 sections of the HRSG and the set 'J', with 3 elements 'j', is used to identify the different pressure  
 351 levels. Also, a set 'K', with 78 elements 'k', is declared to number the process streams associated with  
 352 the *water/steam* working fluid. Thus, each heat exchanger is identified by a 3-tuple (i,j,k). As  
 353 explained later, the element k is important to properly associate streams with heat exchangers. It  
 354 should be noticed that the streams associated with the *gas* working fluid can be numbered using the set  
 355 I already defined to identify the sections of the HRSG. Figure 3a shows the representation of a generic  
 356 section i of the HRSG with a heat exchanger at each pressure level j (LP, MP, HP) with the used  
 357 nomenclature, and Fig. 3b shows how it is instantiated for the section i=13. As illustrated, the three  
 358 (candidate) heat exchangers located in the section i=13 are identified by the following 3-tuples  
 359 (13,LP,1), (13,MP,13), and (13,HP,35). Now, an element k is linked to a specific heat exchanger, so it  
 360 is convenient to define a subset HE that properly links elements k with elements i and j. That is, in Fig.

361 3b, the elements  $k=1$ ,  $k=13$ , and  $k=35$  correspond only to section  $i=13$  and not to the rest of the  
 362 sections. In this way, the subset HE contains all heat exchangers (31 heat exchangers) through the  
 363 correspondence between  $i$ ,  $j$ , and  $k$ . Finally, it is important to note that the evaporators are fixed in the  
 364 superstructure and, therefore, no discrete decisions are associated with them. Then, a new subset EV is  
 365 defined for evaporators in terms of set I. Thus, EV contains the three evaporators located in the  
 366 sections  $i=3, 7, 11$ .

### 367 Insert Figure 3

#### 368 4.1.1 Energy balances

369 Equation (1) calculates the heat load in a heat exchanger in the HRSG (in terms of the  
 370 water/steam working fluid).

$$371 \quad Q_{i,j} = m_{k+1}h_{k+1} - m_k h_k \quad i, j, k \in HE(i, j, k) \quad (1)$$

Then, the energy balance in each section  $i$  is expressed as follows:

$$372 \quad \sum_{j \in HE(i,j,k)} Q_{i,j} = m^G (h_i^G - h_{i+1}^G) \quad \forall i \quad (2)$$

#### 373 4.1.2 Heat transfer area

374 The heat transfer area  $A_{i,j}$  required by the heat exchanger ' $i,j,k$ ' is calculated as follows:

$$375 \quad Q_{i,j} = U_{i,j} A_{i,j} \Delta T_{i,j} \quad i, j \in HE(i, j, k) \quad (3)$$

376 where  $Q_{i,j}$ ,  $U_{i,j}$ , and  $\Delta T_{i,j}$  refer to the heat load, the overall heat transfer coefficient, and the driving  
 377 force, respectively.

378 The Chen approximation (Chen (1987) [49]) (Eq. (4)) is used instead of the logarithmic mean  
 379 temperature difference (LMTD), because it facilitates the model convergence when a heat exchanger is  
 380 removed from the superstructure.

$$381 \quad \Delta T_{i,j} = \sqrt[3]{0.5(T_i^G - T_{k+1})(T_{i+1}^G - T_k) \left[ (T_i^G - T_{k+1}) + (T_{i+1}^G - T_k) \right]} \quad i, j, k \in HE(i, j, k) \quad (4)$$

#### 382 4.2 Logical constraints to select economizers and superheaters

383 In order to select or remove a heat exchanger located in the section  $i$  at the pressure level  $j$ , the  
 384 following two-term disjunction, expressed in terms of the Boolean variable  $X_{i,j}$ , is proposed:  
 385

$$\begin{bmatrix} X_{i,j} \\ Q_{i,j} \leq |Q_{i,j}|_{up} \\ Q_{i,j} \geq |Q_{i,j}|_{lo} \end{bmatrix} \vee \begin{bmatrix} \neg X_{i,j} \\ Q_{i,j} = 0 \end{bmatrix} \quad i, j \in HE(i, j, k) \wedge i \notin EV(i) \quad (D1)$$

386

387 The Boolean variable  $X_{i,j}$  establishes whether a given term in the disjunction is TRUE or  
 388 FALSE. The disjunction D1 states that, if  $X_{i,j}$  is TRUE, then the optimal value of the variable  $Q_{i,j}$  is  
 389 lower than  $|Q_{i,j}|_{up}$  (upper bound) and higher than  $|Q_{i,j}|_{lo}$  (lower bound); consequently,  $A_{i,j} \neq 0$  due to  
 390 Eq. (3). Otherwise, if  $X_{i,j}$  is FALSE, then  $Q_{i,j} = 0$  and, consequently,  $A_{i,j} = 0$ . The disjunction D1 does  
 391 not apply for the subset EV ( $i=3, 7, 11$ ) because it contains the three evaporators that are fixed in the  
 392 superstructure. Then, by associating the binary variable  $x_{i,j}$  with the Boolean variable  $X_{i,j}$  and applying  
 393 Big-M reformulations, the proposed disjunction is translated into the following two algebraic  
 394 inequality constraints:

$$Q_{i,j} \leq x_{i,j} |Q_{i,j}|_{up} \quad i, j \in HE(i, j, k) \wedge i \notin EV(i) \quad (5)$$

$$Q_{i,j} \geq x_{i,j} |Q_{i,j}|_{lo} \quad i, j \in HE(i, j, k) \wedge i \notin EV(i) \quad (6)$$

395 As explained, if  $x_{i,j} = 0$ , then  $Q_{i,j} = 0$  and, consequently,  $A_{i,j} = 0$ . Otherwise, if  $x_{i,j} = 1$ , then  $Q_{i,j}$  is in  
 396 between  $|Q_{i,j}|_{lo}$  and  $|Q_{i,j}|_{up}$  and, consequently,  $A_{i,j} \neq 0$ .

397 Disjunctions similar to D1 are proposed to select pumps and the location of the inlet of the  
 398 steam stream for reheating, as described later.

399

#### 400 4.2.1 Logical constraints to avoid equivalent solutions

401 Equivalent solutions can be frequently obtained when a superstructure-based model is proposed  
 402 for optimization. That is, although the obtained values of the binary variables are different, it is  
 403 possible to obtain optimal solutions that represent the same process configuration. Certainly, the  
 404 superstructure proposed in Fig. 2 embeds several equivalent solutions when superheaters and/or  
 405 economizers are removed from the superstructure.

406

407 Figure 4 shows three equivalent solutions that may be obtained when only one low-pressure  
 408 (LP) superheater is selected. It can be observed that the same resulting heat transfer process can be  
 409 represented by selecting the superheater of either the section  $i=6$  ( $x_{6,LP}=1, x_{5,LP}=0, x_{4,LP}=0$  in Fig. 4a),  
 410 or section  $i=5$  ( $x_{6,LP}=0, x_{5,LP}=1, x_{4,LP}=0$  in Fig. 4b), or section  $i=4$  ( $x_{6,LP}=0, x_{5,LP}=0, x_{4,LP}=1$  in Fig. 4c).

Thus, the same values of heat transfer area, driving force, and amount of heat transferred between the streams #9 and #4 can be obtained by several combinations of the binary variables.

Other equivalent solutions can be obtained if two heat exchangers of the same type are selected. As shown in Fig. 5, in both configurations, the first heat exchange between the gas and water streams takes place at the MP level and the second one at the LP level. Thus, the same resulting configuration can be represented by two different sets of binary variable values ( $x_{6,LP}=1, x_{5,MP}=1, x_{4,LP}=x_{4,MP}=x_{4,HP}=0$  in Fig. 5a, and  $x_{6,LP}=x_{6,MP}=x_{6,HP}=0, x_{5,LP}=1, x_{4,MP}=1$  in Fig. 5b).

In order to avoid the occurrence of the equivalent solutions described in Figs. 4 and 5, it is proposed to select the heat exchangers from left to right, or equivalently, to remove them from right to left. To model this, the following logic propositions are imposed for two successive heat exchangers.

$$\neg\left(\bigvee_{j \in HE(i,j,k)} X_{i,j}\right) \Rightarrow \neg\left(\bigvee_{j \in HE(i-1,j,k)} X_{i-1,j}\right) \quad i = 13, 10, 9, 6, 5, 2 \quad (D2)$$

As presented, the logic propositions apply to the sections  $i=13, 10, 9, 6, 5$ , and 2, establishing that if no heat exchanger is selected in the section  $i$ , then no heat exchanger is selected in the previous section  $i-1$ . This logical proposition can be translated into the following algebraic inequality constraints (Eqs. (7)–(11)):

$$x_{i,LP} + x_{i,MP} + x_{i,HP} + 1 - x_{i-1,LP} \geq 1 \quad i = 13, 10, 9, 6, 5 \quad (7)$$

$$x_{i,LP} + x_{i,MP} + x_{i,HP} + 1 - x_{i-1,MP} \geq 1 \quad i = 13, 10, 9, 6, 5 \quad (8)$$

$$x_{i,LP} + x_{i,MP} + x_{i,HP} + 1 - x_{i-1,HP} \geq 1 \quad i = 13, 10, 9, 6, 5 \quad (9)$$

According to Eqs. (7)–(9), if  $x_{i,LP} = x_{i,MP} = x_{i,HP} = 0$ , then  $x_{i-1,LP} = x_{i-1,MP} = x_{i-1,HP} = 0$ . Also, it can be observed that if  $x_{i,LP} = 1$  or  $x_{i,MP} = 1$  or  $x_{i,HP} = 1$  or  $x_{i,LP} = x_{i,MP} = x_{i,HP} = 1$ , then  $x_{i-1,LP}, x_{i-1,MP}$ , and  $x_{i-1,HP}$  can be individually 0 or 1. These three constraints apply to the sections that involve the three pressure levels. Since no low-pressure level is involved in the section  $i=2$ , the following constraints apply in this case:

$$x_{i,MP} + x_{i,HP} + 1 - x_{i-1,MP} \geq 1 \quad i = 2 \quad (10)$$

$$x_{i,MP} + x_{i,HP} + 1 - x_{i-1,HP} \geq 1 \quad i = 2 \quad (11)$$

However, it should be mentioned that no equivalent solutions can be obtained if three heat exchangers are selected, as illustrated in Fig. 6. In this case, the order in which the gas and water/steam streams exchange heat in Fig. 6a is different from that in Fig. 6b.

#### 4.2.2. Selection of the location and configuration of the reheating process

436 A similar disjunction to D1 is here proposed to select the steam stream that comes from the HP  
 437 steam turbine ST1 for reheating. As shown in Fig. 2, the steam for reheating that comes from ST1 can  
 438 be fed through five candidate streams (#53 to #57). The disjunction D3 is proposed in terms of the  
 439 Boolean variable  $Z_k$ .

$$\begin{bmatrix} Z_k \\ m_k \leq |m_k|_{up} \\ m_k \geq |m_k|_{lo} \end{bmatrix} \vee \begin{bmatrix} \neg Z_k \\ m_k = 0 \end{bmatrix} \quad 53 \leq k \leq 57 \quad (D3)$$

440 As established in D3, if  $Z_k$  is TRUE, then the optimal value of the variable  $m_k$  is lower than  
 441  $|m_k|_{up}$  (upper bound) and higher than  $|m_k|_{lo}$  (lower bound); consequently,  $m_k \neq 0$ . Otherwise, if  $Z_k$  is  
 442 FALSE, then  $m_k = 0$ . Then, by associating the binary variable  $z_k$  with the Boolean variable  $Z_k$ , D3 is  
 443 translated into the following two algebraic inequality constraints:

$$m_k \leq z_k |m_k|_{up} \quad 53 \leq k \leq 57 \quad (12)$$

$$m_k \geq z_k |m_k|_{lo} \quad 53 \leq k \leq 57 \quad (13)$$

444 As a first approximation, only one of these candidate streams can be selected, what is imposed  
 445 through the logical proposition D4, which leads to the algebraic constraint given by Eq. (14):

$$Z_{53} \vee Z_{54} \vee Z_{55} \vee Z_{56} \vee Z_{57} \quad (D4)$$

$$\sum_{k=53}^{57} z_k = 1 \quad (14)$$

### 446 447 4.2.3 Selection of the working fluid pumps

448 A similar disjunction to D1 is also proposed to select the required pumps (D5). As shown, a  
 449 pump is selected in terms of the associated flowrate value. If a pump is not selected, then the  
 450 associated inlet flow is zero.

$$\begin{bmatrix} Y_n \\ m_k \leq |m_k|_{up} \\ m_k \geq |m_k|_{lo} \end{bmatrix} \vee \begin{bmatrix} \neg Y_n \\ m_k = 0 \end{bmatrix} \quad n, k \in PUMP(n, k, k') \wedge n \leq 9 \quad (D5)$$

451  
452 Then, by associating the binary variable  $y_k$  with the Boolean variable  $Y_n$ , D5 is translated into  
 453 the following two algebraic inequality constraints:

$$m_k \leq y_n |m_k|_{up} \quad n, k \in PUMP(n, k, k') \wedge n \leq 9 \quad (15)$$



$$m_k \geq y_n |m_k|_{lo} \quad n, k \in PUMP(n, k, k') \wedge n \leq 9 \quad (16)$$

454

455 For instance, in Fig. 2, if the value of the binary variable associated to the pump #9 ( $y_9$ ) is zero,  
456 then Eqs. (15) and (16) force the associated flow to be zero ( $m_{77} = 0$ ), which is equivalent to  
457 eliminating the pump from the solution.

458 On the other hand, the feed inlet to the MP and HP levels may optionally come from the  
459 condenser or from an inferior pressure level (i.e. MP from LP and HP from MP), as is shown in Fig. 2.  
460 Propositions D6 and D7 are included in the model in order to select a unique feed pump at the MP and  
461 HP levels, which lead to the algebraic constraints given by Eqs. (17) and (18):

$$Y_1 \vee Y_2 \vee Y_9 \quad (D6)$$

$$Y_3 \vee Y_4 \vee Y_5 \vee Y_6 \vee Y_7 \vee Y_8 \quad (D7)$$

$$y_1 + y_2 + y_9 = 1 \quad (17)$$

$$y_3 + y_4 + y_5 + y_6 + y_7 + y_8 = 1 \quad (18)$$

#### 462 4.2.4 Logical constraints between heat exchangers and pumps

463 It is interesting to note that there are also logical relationships between candidate heat  
464 exchangers and candidate pumps that may lead to equivalent solutions when deciding the presence (or  
465 absence) of pumps by solving the proposed superstructure-based optimization model. To avoid the  
466 occurrence of these equivalent solutions, the following two considerations are made.

467 *Consideration 1:* if there is no economizer feeding the pump, then the pump does not exist (proposition  
468 D8). The Boolean variable  $Y_n$  represents the existence of the pump 'n'. The subset NHNP relates the  
469 economizer '(i,j)' to the pump 'n'.

$$\neg X_{i,j} \Rightarrow \neg Y_n \quad \forall i, j, n \in NHNP(i, j, n) \quad (D8)$$

470 Then, the logical proposition D8 is translated into the algebraic constraint given by Eq. (19):

$$x_{i,j} + 1 - y_n \geq 1 \quad \forall i, j, n \in NHNP(i, j, n) \quad (19)$$

471 *Consideration 2:* if a certain economizer exists, then there are no pumps after it at the inferior pressure  
472 level (proposition D9). The HNP subset relates the exchanger '(i,j)' to the pump 'n'.

$$X_{i,j} \Rightarrow \neg Y_n \quad \forall i, j, n \in HNP(i, j, n) \quad (D9)$$

473 The logical proposition D9 is translated into the algebraic constraint given by Eq. (20):

$$1 - x_{i,j} + 1 - y_n \geq 1 \quad \forall i, j, n \in HNP(i, j, n) \quad (20)$$

474 In this way, Eqs. (15)–(20) allow an orderly elimination by relating the heat exchangers and the  
475 associated pumps as appropriate.

476

477 **4.2.5 Possibility of selecting parallel heat exchangers**

478 As mentioned earlier, the HRSG superstructure also includes the possibility of selecting heat  
 479 exchangers operating in parallel at each section of the HRSG, except for the sections that contain  
 480 evaporators. This possibility is allowed by the following constraint:

$$\sum_{j \in HE(i,j,k)} x_{i,j} \leq PE_i \quad i \notin EV(j) \quad (21)$$

481 where  $PE_i$  refers to the maximum number of heat exchangers operating in parallel at the section  $i$ ; it is  
 482 a model parameter that can be varied.

483

484 **4.2.6 Possibility of limiting the number of economizers and superhetars at each pressure level**

485 In addition, the model includes constraints related to the maximum number of economizers  $EC_j$   
 486 (Eq. (22)) and superheaters  $SH_j$  (Eq. (23)) that are allowed to operate at each pressure level  $j$  (LP, MP,  
 487 and HP):

$$\sum_{i \in EC(i,j)} x_{i,j} \leq EC_j \quad \forall j \quad (22)$$

$$\sum_{i \in SH(i,j)} x_{i,j} \leq SH_j \quad \forall j \quad (23)$$

488  $EC_j$  and  $SH_j$  are model parameters that can be varied.

489

490 **4.3 Calculation of the physical-chemical properties**

491 The use of dynamic-link libraries (DLLs) as well as extrinsic functions allows to significantly  
 492 enhance the model implementation compared to the traditional approach, and to considerably reduce  
 493 the model size as well as the computational time required by the optimization algorithms. For instance,  
 494 a MINLP model to optimize the process configuration of two coupled distillation columns including  
 495 DLLs and extrinsic functions required almost 4000 constraints and variables less than if no DLLs and  
 496 extrinsic functions are employed (Manassaldi et al. 2019). In addition, the time required to solve the  
 497 NLP models was less than half in comparison with models without employing DLLs and extrinsic  
 498 functions.

499

500 **4.4 Objective function**

501 The optimization criterion is the minimization of the total heat transfer area (THTA) which is  
 502 calculated in Eq. (24):

$$THTA = \sum_{i,j \in HE(i,j,k)} A_{i,j} + A_{COND} \quad (24)$$

where  $A_{COND}$  refers to the heat transfer area of the condenser in the Rankine cycle.

## 5. Discussion of results

The results discussed in this section correspond to the performed model verification and the obtained optimal solutions.

Tables 1 and 2 list the numerical values of the model parameters and the lower and upper bounds, respectively, used for all optimizations.

**Table 1.** Values of model parameters used in all case studies.

| Flue gas specification                           |                      | Source |                             |
|--|----------------------|--------|-----------------------------|
| Mass flow rate of gas turbine exhaust gases      | kg/s                 | 445.4  | (Franco and Giannini, 2006) |
| Temperature of gas turbine exhaust gases         | K                    | 778.15 | (Franco and Giannini, 2006) |
| Minimum outlet temperature of gases leaving HRSG | K                    | 348.15 | (Franco and Giannini, 2006) |
| Process units                                    |                      |        |                             |
| Economizer overall heat transfer coefficient     | W/(m <sup>2</sup> K) | 42.60  | (Franco and Russo, 2002)    |
| Evaporator overall heat transfer coefficient     | W/(m <sup>2</sup> K) | 43.70  | (Franco and Russo, 2002)    |
| Superheater overall heat transfer coefficient    | W/(m <sup>2</sup> K) | 50.00  | (Franco and Russo, 2002)    |
| Minimum pinch point                              | K                    | 10.00  | (Franco and Giannini, 2006) |
| Minimum heat transfer temperature difference     | K                    | 10.00  | (Franco and Giannini, 2006) |
| Condenser pressure                               | bar                  | 0.1733 | (Franco and Giannini, 2006) |
| Isentropic efficiency of steam turbines          | dimensionless        | 0.90   | (Franco and Russo, 2002)    |
| Efficiency of pumps                              | dimensionless        | 0.75   | (Manassaldi et al., 2016)   |

**Table 2.** Lower and upper bounds on optimization variables used in all case studies.

| Variable                     |      | Lower bound | Upper bound |
|------------------------------|------|-------------|-------------|
| High pressure ( $P^{HP}$ )   | bar  | 110         | 180*        |
| Medium pressure ( $P^{MP}$ ) | bar  | 10          | 60          |
| Low pressure ( $P^{LP}$ )    | bar  | 1           | 10          |
| Temperature (T)              | K    | 330.15*     | 768.15*     |
| Mass flow rate (m)           | kg/s | 0           | 100         |

\* Value taken from Franco and Giannini (2006).

The proposed mathematical model involves 588 continuous variables, 42 binary variables, and 773 constraints (equality and inequality constraints) and was implemented in GAMS 23.9.5 (General Algebraic Modeling System). SBB (Standard Branch and Bound) (Bussieck and Drud, 2001) and CONOPT (Drud, 1992) are the solvers used for the mixed-integer nonlinear problems (MINLP) and nonlinear problems (NLP), respectively. SBB is employed because it is suitable for solving models that have fewer discrete decisions but more difficult nonlinearities ([https://www.gams.com/latest/docs/S\\_SBB.html#SBB\\_COMPARISON\\_OF\\_DICOT\\_AND\\_SBB](https://www.gams.com/latest/docs/S_SBB.html#SBB_COMPARISON_OF_DICOT_AND_SBB)), characteristics involved by the model proposed in this work.

523 In the current model, DLLs are used to calculate the enthalpy, entropy, specific volume, and  
 524 density of the working fluid of the steam cycle (water, steam). As shown in Fig. 7, extrinsic functions  
 525 associated to the correlations reported in ‘Revised Release on the IAPWS Industrial Formulation 1997  
 526 for the Thermodynamic Properties of Water and Steam’ (IAPWS R7-97, 2012) are declared in the C  
 527 programming language in a DevC++ project generating the corresponding DLLs (extrinsic.DLL),  
 528 which are included in GAMS (\$funclibin IAPWS iapws.dll) and executed outside GAMS.

529 In the file *extrfunc.h* all the definitions required to create the libraries are included. In the file  
 530 *mylibraryql.c* the architectures of the library and the functions are defined. Finally, in the *mylibrary.c*  
 531 the functions are programmed and/or imported. As illustrated in Fig. 7, for each  
 532 physicochemical property an extrinsic function has been declared. A detailed description about the  
 533 implementation of DLLs for all physicochemical properties and how they interact with GAMS can be  
 534 found in Manassaldi et al. (2019). The IAPWS.dll library is available and can be downloaded from the  
 535 GAMS World Forum (<https://forum.gamsworld.org/viewtopic.php?f=16&t=11547>). The model  
 536 involves many nonlinear constraints. For instance, the domains of many functions from the IAPWS-  
 537 IF97 are nonconvex (Bongartz et al., 2020). Also, bilinear terms appearing in the energy balances as  
 538 well as in the design equations used to calculate the heat transfer areas of all heat exchangers are  
 539 involved.

## 541 5.1 Model verification

542 The proposed model was successfully verified by comparing the model output with the optimal  
 543 solution presented in Franco and Giannini (2006), whose optimal process configuration – hereafter  
 544 referred as the ‘RC configuration’ – is illustrated in Fig. 8. In order to perform a correct verification  
 545 and because the MINLP model developed in this work embeds many candidate configurations, several  
 546 (discrete and continuous) model variables were fixed at the optimal values reported for the RC  
 547 configuration. Then, an optimization problem consisting in the minimization of the sum of the  
 548 square errors between the data taken from Franco and Giannini (2006) and the values calculated by the  
 549 model (Eq. (25)), was solved:

$$550 \text{Min} \left( \sum_{k \in MK(k)} (m_k^{FG} - m_k)^2 + \sum_{k \in PK(k)} (P_k^{FG} - P_k)^2 + \sum_{k \in TK(k)} (T_k^{FG} - T_k)^2 + \sum_{(i,j) \in QK(i,j)} (Q_{i,j}^{FG} - Q_{i,j})^2 \right) \quad (25)$$

551

552 where the subscript **FG** refers to data reported by Franco and Giannini (2006); the subsets **MK**,  
 553 **PK**, **TK** contain the stream  $k$  with mass flow rate  $m_k$ , pressure  $P_k$ , temperature  $T_k$ , respectively. The  
 554 subset **QK** contains the heat load  $Q$  of the heat exchanger  $i,j$ .

555 Table 3 compares the values of pressure, temperature, and mass flow rate of the streams of the  
 556 circulating fluid in the Rankine cycle. Table 4 compares the gas stream temperatures. Table 5  
 557 compares the values of the total heat load in the HRSG and in each heat exchanger. The values that  
 558 were fixed in the MINLP model and that are used in Eq. (25) are marked with the symbol \* in these  
 559 tables. The remaining variables listed in the tables are the outputs used for comparison. The three  
 560 tables include the percentage error computed for each variable.

561

562 **Table 3.** Comparison of the pressure, temperature, and mass flow rate values of the streams of  
 563 the circulating fluid in the Rankine cycle reported by Franco and Giannini (2006) and the obtained in  
 564 this work (MINLP model).

| Stream # of the working<br>fluid in the Rankine<br>cycle | Franco and Giannini (2006) |       |          | This work |        |          | Error (%) |        |          |
|--|----------------------------|-------|----------|-----------|--------|----------|-----------|--------|----------|
|  | P (bar)                    | T (K) | m (kg/s) | P (bar)   | T (K)  | m (kg/s) | P (bar)   | T (K)  | m (kg/s) |
| 6  | 6.0                        | 432.0 | 13.62    | 6.0*      | 432.0  | 13.62*   | 0.00%     | 0.02%  | 0.00%    |
| 12   | 6.0                        | 501.1 | 13.62    | 6.0       | 501.1* | 13.62*   | 0.00%     | 0.00%  | 0.00%    |
| 18   | 53.0                       | 501.1 | 45.79    | 54.387    | 501.1* | 45.801   | -2.62%    | 0.00%  | -0.02%   |
| 24   | 53.0                       | 540.7 | 15.33    | 54.387    | 542.4  | 15.353   | -2.62%    | -0.31% | -0.15%   |
| 26   | 53.0                       | 603.1 | 15.33    | 54.387    | 603.4  | 15.353   | -2.62%    | -0.05% | -0.15%   |
| 28   | 53.0                       | 624.9 | 45.79    | 54.387    | 624.9  | 45.801   | -2.62%    | 0.00%  | -0.02%   |
| 34   | 53.0                       | 768.1 | 45.79    | 54.387    | 768.1  | 45.801   | -2.62%    | 0.00%  | -0.02%   |
| 49   | 169.0                      | 624.9 | 30.46    | 168.525   | 624.7  | 30.449   | 0.28%     | 0.04%  | 0.04%    |
| 51   | 169.0                      | 768.1 | 30.46    | 168.525   | 768.1* | 30.449   | 0.28%     | 0.00%  | 0.04%    |
| 75   | 0.1733                     | 330.1 | 59.41    | 0.1733*   | 330.1* | 59.421   | 0.00%     | 0.00%  | -0.02%   |

565 \* Numerical values fixed in the MINLP model that are used in Eq. (25).

566

567 **Table 4.** Comparison of the temperature values of the gas streams reported by Franco and Giannini  
 568 (2006) and the obtained in this work (MINLP model).

| Stream # of gas | $T^G$ (K)                  |           |           |
|-----------------|----------------------------|-----------|-----------|
|                 | Franco and Giannini (2006) | This work | Error (%) |
| 1               | 778.1                      | 778.1 *   | 0.00%     |
| 3               | 702.6                      | 704.4     | -0.26%    |
| 4               | 651.1                      | 652.7     | -0.24%    |
| 6               | 634.9                      | 636.7     | -0.27%    |
| 7               | 607.8                      | 610.0     | -0.36%    |

|    |       |       |        |
|----|-------|-------|--------|
| 8  | 558.1 | 560.7 | -0.46% |
| 10 | 540.8 | 542.3 | -0.27% |
| 11 | 508.3 | 509.5 | -0.23% |
| 12 | 450.3 | 451.5 | -0.26% |
| 14 | 395.6 | 398.5 | -0.72% |

\* Numerical value fixed in the MINLP model that are used in Eq. (25).

**Table 5.** Comparison of the values of the total heat load in the HRSG and in each heat exchanger reported by Franco and Giannini (2006) and the obtained in this work (MINLP model).

|                      | Heat load (MW)             |               |             |
|----------------------|----------------------------|---------------|-------------|
|                      | Franco and Giannini (2006) | This work     | Error (%)   |
| <b>Total</b>         | <b>191.43</b>              | <b>190.23</b> | <b>0.63</b> |
| Heat exchanger (i,j) |                            |               |             |
| (13,LP)              | 26.24                      | 25.63         | -2.36       |
| (10,MP)              | 14.14                      | 14.11         | -0.21       |
| (9,MP)               | 8.59                       | 9.15          | 6.16        |
| (6,HP)               | 10.5                       | 10.19         | -3.04       |
| (5,HP)               | 5.09                       | 5.19          | 2.00        |
| (11,LP)              | 28.39                      | 28.41         | 0.06        |
| (7,MP)               | 24.86                      | 24.70         | -0.64       |
| (3,HP)               | 26.29                      | 26.45         | 0.60        |
| (10,LP)              | 1.95                       | 2.11          | 7.61        |
| (6,MP)               | 3.16                       | 3.26          | 3.11        |
| (5,MP)               | 3.12                       | 2.93          | -6.57       |
| (2,MP)               | 17.24                      | 16.23         | -6.20       |
| (2,HP)               | 21.86                      | 21.86         | -0.01       |

According to the values listed in Tables 3 and 4, the maximum deviation is  $-2.62\%$ , which corresponds to the pressure of stream #18. This deviation may be due to the fact that the correlations used by Franco and Giannini (2006) to estimate the enthalpy and vapor pressure values of the circulating fluid at different conditions (superheated and saturated steam, subcooled and saturated liquid) are different from those used in this study. The deviations in the rest of the variables are practically insignificant. Regarding the deviations computed for heat loads, it can be seen in Table 5 that the deviation in the total heat load in the HRSG is only  $0.63\%$  (191.43 MW vs. 190.23 MW), with the particularity that the calculated values for some heat exchangers are higher than those reported by Franco and Giannini (2006), but for others they are lower. However, the variations along the HRSG compensate, resulting in a total deviation of  $0.63\%$ . Then, based on the obtained percentage deviations, it can be concluded that, for the purpose of this study, the implemented process model successfully predicts the solution reported by Franco and Giannini (2006).

## 5.2 Optimization results

This section presents the optimization results obtained by solving the problem stated in Section 3, which consists in determining the optimal configuration of the heat exchangers with their corresponding sizes and operating conditions that minimize the total heat transfer area of the HRSG to generate a fixed, specified total net power. For comparison purpose, it is specified the total net power value calculated in Franco and Giannini (2006) (RC configuration), which is equal to 63.026 MW. The obtained optimal solution is hereafter named ‘OS’.

For all optimization cases, the numerical values of the model parameters and bounds on decision variables are the same as those listed in Tables 1 and 2. In addition, the model has been solved by setting the option *optcr* at the minimum value supported by the solver ( $1.0 \times 10^{-9}$ ). To obtain the integer solution of this case study, the optimization algorithm explored 34 nodes and stopped with a relative gap of  $9.34 \times 10^{-16}$  requiring 3773 iterations and 23.32 NLP seconds.

Figure 9 illustrates the optimal configuration corresponding to OS and Fig. 10 compares the T-H diagrams resulting from the RC and OS solutions. Tables 6–10 compare the optimal values obtained for both RC and OS solutions.

**Table 6.** Comparison of optimal values obtained for RC and OS solutions (gas temperature, total heat load, and total heat transfer area in each HRSG zone).

| Point | HRSG zone         | Gas temperature (K) |       | Heat load (MW)    |                   | Heat transfer area ( $\times 10^3 \text{ m}^2$ ) |              |
|-------|-------------------|---------------------|-------|-------------------|-------------------|--|--------------|
|       |                   | RC                  | OS    | RC                | OS                | RC   | OS           |
| 1     | Hot zone          | 778.1               | 778.1 | 64.54             | <b>68.57</b>      | 35.40  | <b>25.65</b> |
| 2     |                   | 778.1               | 745.8 | (3 HEXs)          | (5 HEXs)          |  |              |
| 3     |                   | 704.5               | 710.0 | 2,HP/2,MP/3,HP    | 1,HP/1,MP/2,HP    |  |              |
| 4     |                   | 652.7               | 644.7 |                   | 2,MP/3,HP         |  |              |
| 5     | Intermediate zone | 652.7               | 642.7 | 46.27             | <b>62.25</b>      | 27.17  | <b>30.36</b> |
| 6     |                   | 636.7               | 578.2 | (5 HEXs)          | (6 HEXs)          |  |              |
| 7     |                   | 610.0               | 572.8 | 5,HP/5,MP/6,HP/   | 4,MP/5,HP/5,MP/   |  |              |
| 8     |                   | 560.7               | 520.4 | 6,MP/7,MP         | 6,MP/6,LP/7,MP    |  |              |
| 9     |                   | 560.7               | 520.4 |                   |                   |  |              |
| 10    | Cold zone         | 542.3               | 520.4 | 79.41             | <b>61.31</b>      | 45.13  | <b>35.72</b> |
| 11    |                   | 509.5               | 482.7 | (5 HEXs)          | (7 HEXs)          |  |              |
| 12    |                   | 451.5               | 438.2 | 9,MP/10,MP/       | 10,HP/10,MP/10,LP |  |              |
| 13    |                   | 451.5               | 438.2 | 10,LP/11,LP/13,LP | 11,LP/13,HP/      |  |              |
| 14    |                   | 398.6               | 394.5 |                   | 13,MP/ 13,LP      |  |              |
|       |                   |                     |       | <b>190.23</b>     | <b>192.14</b>     | <b>107.70</b>                                    | <b>91.74</b> |

Figures 8 and 9 clearly show the differences that exist between the configuration reported by Franco and Giannini (2006) (RC) and the optimal configuration obtained by the proposed model (OS). As can be seen in Fig. 9, the optimal number of heat exchangers in OS is 18, i.e., 5 heat exchangers more than in RC (Fig. (8)). According to the results listed in Tables 6 and 7, it can be observed that the

609 total heat exchanged between the gas and the circulating fluid in the hottest zone of the HRSG  
610 (sections  $i = 1-3$ ) is similar (64.54 MW in RC vs. 68.57 MW in OS) because the difference in the gas  
611 outlet temperature in this zone ( $i = 3$ ) – which is an optimization variable of the model – only differs in  
612 8 K (652.7 K in RC vs. 644.7 K in OS, Table 6). While the gas inlet temperature and flow rate in the  
613 section  $i = 1$  are the same in both configurations since, as mentioned above, they are fixed and known  
614 values – i.e. model parameters – taken from Franco and Giannini (2006). Although in the hot zone the  
615 total heat exchanged in OS is slightly higher than in RC (4.03 MW according to Table 7), the area  
616 required in OS is 27.54 % lower than that required in RC (25650 m<sup>2</sup> vs. 35400 m<sup>2</sup>), which is obtained  
617 using 2 heat exchangers more than in RC, specifically two superheaters (1,HP) and (1,MP) at the high  
618 and medium pressure levels, respectively. In the OS configuration (Fig. 9), in addition to the  
619 evaporator EV1 ( $i = 3$ ), sections  $i = 1$  and 2 involve 4 heat exchangers in total, with 2 exchangers in  
620 each section, where the gas stream exchanges heat in parallel with the circulating fluid at MP and HP  
621 levels. On the other hand, in the RC configuration (Fig. 8), there are only 2 parallel heat exchangers,  
622 precisely in the section  $i = 2$ . The fact of using 4 heat exchangers in OS – not 2 as in RC – allows to  
623 increase the degrees of freedom of the optimization problem since it is possible to conveniently vary,  
624 not only the temperature of both the gas stream and circulating fluid, but also the corresponding flow  
625 rates, in such a way that the heat transfer area in OS is smaller than in RC to transfer practically the  
626 same amount of total heat in this zone of the HRSG. According to the values listed in Table 7 for OS,  
627 the heat exchangers selected in the MP and HP levels in the section  $i = 2$  ((2,MP) and (2,HP)) require  
628 1530 m<sup>2</sup> and 3000 m<sup>2</sup>, respectively, to transfer 6.11 MW and 12.37 MW, with a driving force of 80.04  
629 K and 82.47 K, respectively. While for RC, Table 7 shows that these two heat exchangers require 9870  
630 m<sup>2</sup> and 13260 m<sup>2</sup> to transfer 16.23 MW and 21.86 MW, respectively, with a driving force of 32.90 K  
631 and 32.95 K. In the section  $i = 1$ , the heat exchangers (1,MP) and (1,HP) selected in OS require 3270  
632 m<sup>2</sup> and 3950 m<sup>2</sup>, respectively, to transfer 7.71 MW and 9.04 MW with a driving force of 47.17 K and  
633 45.81 K. The section  $i = 3$  involves the evaporator (3,HP), which is fixed in the superstructure i.e. it is  
634 not a decision variable, as mentioned in the model presentation. The heat transfer area required by  
635 (3,HP) in OS is 1630 m<sup>2</sup> larger than in RC, transferring 6.87 MW more than in RC (33.32 MW vs.  
636 26.45 MW) with a driving force 5.51 K greater (54.84 K in OS vs. 49.33 K in RC). The operating  
637 temperature in (3,HP) – which corresponds to stream #49 of saturated steam in Table 8 – in OS is 8.65  
638 K lower than in RC (616.08 K vs. 624.73 K) and the associated flow rate in OS is 3.185 kg/s higher  
639 (33.634 kg/s vs. 30.449 kg/s). The temperature-enthalpy (T-H) diagrams corresponding to both RC and  
640 OS configurations are compared in Figure 10, which allow visualizing how these variables are



641 influenced by the inclusion of 2 parallel heat exchangers in the section  $i = 1$ , affecting significantly the  
 642 driving forces and the heat transfer areas of the different process units.

643 In the intermediate-temperature zone of the HRSG, consisting of sections  $i = 4-8$ , in addition to  
 644 the evaporator EV2 ( $i=7$ ), the OS configuration includes one heat exchanger more than the RC  
 645 configuration (5 vs. 4) and it shows a different arrangement of the process units and a different  
 646 location of the inlet point of the stream associated with the reheating of the steam coming from the  
 647 turbine ST1. Unlike in the hot zone, the gas outlet temperature in the intermediate zone ( $T_9$  in Table 6)  
 648 is 520.4 K in OS and 560.7 K in RC, resulting in a recovered heat amount and a heat transfer area  
 649 required in OS by around 34.53% and 11.74% higher than in RC, respectively (62.25 MW vs. 46.27  
 650 MW and 30360 m<sup>2</sup> vs. 27170 m<sup>2</sup>, according to Table 7). By comparing Figs. 8 and 9 it can be seen that  
 651 the heat exchanged in parallel between the gas stream and the circulating fluid in the section  $i = 6$  takes  
 652 place at LP and MP levels in OS (i.e. in (6,LP) and (6,MP)); whereas in RC the heat exchanges take  
 653 place at MP and HP levels (i.e. in (6,MP) and (6,HP)). Another difference is the location at which  
 654 steam superheating begins. In the OS configuration (Fig. 9), the steam leaving the turbine ST1 mixes  
 655 with the saturated steam leaving the evaporator (7,MP) (stream #25) and enters the superheater  
 656 (6,MP). Differently, in RC (Fig. 8), the stream leaving the evaporator (7,MP) is first reheated in the  
 657 superheater (6,MP) and then it is mixed with the stream leaving ST1 (stream #25), entering a second  
 658 superheater (5,MP). The T-H diagrams (Fig. 10) show the temperature differences on the hot and cold  
 659 sides of each heat exchanger of both configurations, which determine the corresponding driving forces  
 660 that affect the heat transfer areas. Compared to RC, Fig. 10 and Tables 7 and 8 show that the operating  
 661 temperature in the evaporator (7,MP) in OS is 45.3 K lower (497.13 K vs. 542.40 K, in Table 8), its  
 662 heat load is slightly higher (26.06 MW vs. 24.70 MW, in Table 7) but requiring less heat transfer area  
 663 (13450 m<sup>2</sup> vs. 15030 m<sup>2</sup>, in Table 7) as a result of the temperature differences at the ends of the  
 664 evaporator (23.3 K vs. 18.3 K at the cold end and 75.7 K vs 67.6 K at the hot end), which implies a  
 665 greater driving force (44.3 K vs. 37.6 K, in Table 7). The heat exchanger (6,MP) exhibits a different  
 666 behavior to that observed for (7,MP) since the heat load in OS is 1.17 MW lower than in RC (2.09  
 667 MW vs. 3.26 MW), requiring less heat transfer area (680 m<sup>2</sup> vs. 1350 m<sup>2</sup>) with a driving force of 61.1  
 668 K, which is 12.76 K greater than in RC (48.4 K). However, the heat exchangers (5,HP) and (5,MP)  
 669 exhibit a different behavior from the previous ones (7,MP and 6,MP) since not only the heat loads but  
 670 also the heat transfer areas in OS are greater than those in RC, although the associated driving forces in  
 671 OS are still greater than in RC. Precisely, the heat transfer areas required in OS by (5,HP) and (5,MP)  
 672 are 10510 m<sup>2</sup> and 4830 m<sup>2</sup>, respectively, while those required in RC are 3970 m<sup>2</sup> and 1890 m<sup>2</sup>,  
 673 respectively. From the analysis performed for each section of the intermediate-temperature zone of the

674 HRSG, it is concluded that the transfer area increases of the heat exchangers (6,LP), (5,HP), and  
 675 (5,MP) prevail over those of the heat exchangers (7,MP), (6,HP), and (6,MP), implying an increase of  
 676 the total heat transfer area in OS with respect to RC (30360 m<sup>2</sup> vs. 27170 m<sup>2</sup>).

677

678 **Table 7.** Comparison of solutions obtained for RC and OS configurations (heat load, driving force, and  
 679 heat transfer area values for each heat exchanger and HRSG zone).

| Heat exchanger<br>(‘section’, ‘pressure level’) | HRSG zone         | RC solution   |              |   | OS solution   |              |   |      |
|---|-------------------|---------------|--------------|---|---------------|--------------|---|------|
|   |                   | Q (MW)        | DF (K)       | Area (x10 <sup>3</sup> m <sup>2</sup> ) | Q (MW)        | DF (K)       | Area (x10 <sup>3</sup> m <sup>2</sup> ) |      |
| 1,MP  | Hot zone          | 0             | 10           | 0                                       | 7.71          | 47.17        | 3.27                                    |      |
| 1,HP  |                   | 0             | 10           | 0                                       | 9.04          | 45.81        | 3.95                                    |      |
| 2,MP  |                   | 16.23         | 32.90        | 9.87                                    | 6.11          | 80.04        | 1.53                                    |      |
| 2,HP  |                   | 21.86         | 32.95        | 13.26                                   | 12.37         | 82.47        | 3.00                                    |      |
| 3,HP  |                   | 26.45         | 49.33        | 12.27                                   | 33.32         | 54.84        | 13.90                                   |      |
| <b>Total</b>                                    |                   | <b>64.54</b>  | <b>-</b>     | <b>35.40</b>                            | <b>68.57</b>  | <b>-</b>     | <b>25.65</b>                            |      |
| 4,MP  | Intermediate zone | -             | 27.73        | -                                       | 1.01          | 29.01        | 0.70                                    |      |
| 5,HP  |                   | 5.19          | 30.65        | 3.97                                    | 22.00         | 49.12        | 10.51                                   |      |
| 5,MP  |                   | 2.93          | 30.95        | 1.89                                    | 10.51         | 43.54        | 4.83                                    |      |
| 6,HP  |                   | 10.19         | 48.58        | 4.92                                    | 0             | 79.20        | 0                                       |      |
| 6,LP  |                   | 0             | 121.71       | 0                                       | 0.58          | 62.18        | 0.19                                    |      |
| 6,MP  |                   | 3.26          | 48.39        | 1.35                                    | 2.09          | 61.15        | 0.68                                    |      |
| 7,MP  |                   | 24.70         | 37.62        | 15.03                                   | 26.06         | 44.34        | 13.45                                   |      |
| <b>Total</b>                                    |                   | <b>46.27</b>  | <b>-</b>     | <b>27.17</b>                            | <b>62.25</b>  | <b>-</b>     | <b>30.36</b>                            |      |
| 9,MP  |                   | Cold zone     | 9.15         | 28.20                                   | 7.62          | 0            | 23.26                                   | 0    |
| 10,HP   |                   |               | 0            | 195.31                                  | 0             | 11.70        | 41.54                                   | 6.61 |
| 10,LP   | 2.11              |               | 57.43        | 0.735                                   | 1.79          | 39.50        | 0.91                                    |      |
| 10,MP   | 14.11             |               | 57.43        | 5.77                                    | 5.05          | 40.95        | 2.90                                    |      |
| 11,LP   | 28.41             |               | 41.88        | 15.52                                   | 21.68         | 39.29        | 12.63                                   |      |
| 13,LP   | 25.63             |               | 38.85        | 15.49                                   | 3.73          | 38.82        | 2.25                                    |      |
| 13,MP   | 0                 |               | 92.32        | 0                                       | 5.17          | 39.11        | 3.10                                    |      |
| 13,HP   | 0                 |               | 92.32        | 0                                       | 12.19         | 39.07        | 7.32                                    |      |
| <b>Total</b>                                    | <b>79.41</b>      | <b>-</b>      | <b>45.13</b> | <b>61.31</b>                            | <b>-</b>      | <b>35.72</b> |   |      |
| <b>Condenser</b>                                |                   | 126.31        | 14.36        | 2.58                                    | 128.83        | 14.36        | 2.64                                    |      |
| <b>Total</b>                                    |                   | <b>316.54</b> | <b>-</b>     | <b>110.29</b>                           | <b>320.97</b> | <b>-</b>     | <b>94.37</b>                            |      |

680

681 Finally, when comparing the cold zone of the HRSG (sections  $i = 9-13$ ) between the RC and  
 682 OS configurations (Figs. 8 and 9, respectively), it can be seen that both the number of heat exchangers  
 683 and their configurations, as well as the amount of transferred heat and required transfer area, are  
 684 different. Precisely, the OS and RC configurations require 7 and 5 heat exchangers, respectively, to  
 685 transfer in total 61.31 MW and 79.41 MW, with a total area of 35720 m<sup>2</sup> and 45130 m<sup>2</sup> in each case  
 686 (Tables 6 and 7). It is important to note that, although the temperature of the gas stream leaving the

687 cold zone (section  $i = 13$ , stream #14) in OS is 4.1 K lower than in RC (394.5 vs. 398.6 K), the inlet  
 688 temperature is 40.3 K lower (520.4 K vs. 560.7 K), resulting in a lower total heat load (Table 6).  
 689 Except for the section  $i = 11$ , which consists of an evaporator in both configurations, Fig. 9 shows that  
 690 the remaining sections ( $i = 10, 13$ ) are composed of 3 heat exchangers, in which the gas stream  
 691 exchanges heat in parallel with each of the circulating fluids at the three pressure levels (3 economizers  
 692 in the section  $i = 13$  and 2 economizers and 1 reheater in the section  $i = 10$ ), unlike what is observed in  
 693 Fig. 8 for RC, where only 1 heat exchanger is present in the section  $i = 13$  (economizer) and 2 heat  
 694 exchangers in the section  $i = 10$  (economizer and reheater). Figure 9 clearly shows that the circulating  
 695 fluid stream splits and enters the section  $i = 1$  in OS at the three pressure levels (LP, MP, and HP),  
 696 unlike what happens in RC (Fig. 8), where the circulating fluid stream enters the section  $i = 1$  at the LP  
 697 level only (stream #1). As indicated in Fig. 8 for RC, once the stream #1 is preheated in the  
 698 economizer (13,LP), it is divided into the stream #3, which enters the evaporator (11,LP), and stream  
 699 #58, which starts circulating at the MP level by the pump P1 that is selected from the model.  
 700 Afterward, the stream #20 leaving the economizer (9,MP) is divided into the stream #21, which enters  
 701 the evaporator (7,MP), and stream #65, which starts circulating at the HP level by the pump P6.

702 The T-H diagrams (Fig. 10) allow to see how the temperatures of the circulating fluids  
 703 (water/steam) corresponding to the three pressure levels and the temperatures of the gas stream are  
 704 distributed along the HRGS to transfer the amount of heat needed in each piece of equipment, in order  
 705 to satisfy the total energy balance and obtain the necessary driving forces for a minimal total heat  
 706 transfer area. Comparing the trends shown by the process units that are present in both configurations  
 707 – (13,LP), (11,LP), (10,MP), and (10,LP) –, it can be concluded that, except for exchanger (10,LP), all  
 708 of them have a heat load and an associated transfer area in RC greater than in OS. Differently, the heat  
 709 exchanger (10,LP) presents the highest heat load but the lowest heat transfer area.

711 As a summary of the analysis performed in each zone of the HRSG, it can be concluded that,  
 712 although the total heat loads of the HRSG corresponding to both the RC and OS configurations are  
 713 very similar (190.23 MW and 192.14 MW, respectively), the total heat transfer area required in OS is  
 714 14.82% lower than in RC (91740 m<sup>2</sup> vs. 107700 m<sup>2</sup>). This is due to the inclusion in OS of 4 heat  
 715 exchangers more than in RC, making it possible to modify the RC configuration, include parallel  
 716 exchanges along the HRSG, and obtain more appropriate driving forces (temperature differences at the  
 717 cold and hot sides) in each heat exchanger. Compared to the RC solution, the heat transfer area in the  
 718 hot and cold zones of the HRSG required in the OS solution is 19160 m<sup>2</sup> smaller, but it is 3190 m<sup>2</sup>  
 719 larger in the intermediate-temperature zone, resulting in a net reduction of 15970 m<sup>2</sup> in the HRSG. The

720 results listed in Table 7 corresponding to the condenser indicate that the OS solution requires  
 721 transferring 128.83 MW with an area of 2640 m<sup>2</sup>, compared with 126.31 MW and 2580 m<sup>2</sup>,  
 722 respectively, required in the RC solution.

723 **Table 8.** Comparison of the operating conditions in RC and OS configurations.

| water stream | RC      |        |          | OS      |        |          |
|--------------|---------|--------|----------|---------|--------|----------|
|              | P (bar) | T (K)  | m (kg/s) | P (bar) | T (K)  | m (kg/s) |
| 1            | 6.0     | 330.15 | 59.421   | 4.024   | 330.15 | 10.166   |
| 5            | 6.0     | 431.98 | 13.620   | 4.024   | 416.98 | 10.166   |
| 6            | 6.0     | 431.98 | 13.620   | 4.024   | 416.98 | 10.166   |
| 7            | 6.0     | 501.15 | 13.620   | 4.024   | 498.87 | 10.166   |
| 12           | 6.0     | 501.15 | 13.620   | 4.024   | 526.46 | 10.166   |
| 14           | 54.387  | 330.15 | 0        | 25.01   | 416.60 | 14.166   |
| 18           | 54.387  | 501.15 | 45.801   | 25.01   | 497.13 | 14.166   |
| 23           | 54.387  | 542.40 | 15.353   | 25.01   | 497.13 | 14.166   |
| 24           | 54.387  | 542.40 | 15.353   | 25.01   | 497.13 | 14.166   |
| 25           | 54.387  | 542.40 | 15.353   | 25.01   | 506.78 | 47.80    |
| 26           | 54.387  | 603.44 | 15.353   | 25.01   | 521.70 | 47.80    |
| 27           | 54.387  | 602.27 | 45.801   | 25.01   | 521.70 | 47.80    |
| 28           | 54.387  | 624.95 | 45.801   | 25.01   | 609.98 | 47.80    |
| 31           | 54.387  | 624.95 | 45.801   | 25.01   | 619.16 | 47.80    |
| 32           | 54.387  | 768.15 | 45.801   | 25.01   | 675.74 | 47.80    |
| 34           | 54.387  | 768.15 | 45.801   | 25.01   | 748.23 | 47.80    |
| 36           | 168.525 | 330.15 | 0        | 151.451 | 416.66 | 33.634   |
| 40           | 168.525 | 330.15 | 0        | 151.451 | 496.29 | 33.634   |
| 46           | 168.525 | 603.15 | 30.449   | 151.451 | 496.29 | 33.634   |
| 48           | 168.525 | 624.73 | 30.449   | 151.451 | 616.08 | 33.634   |
| 49           | 168.525 | 624.73 | 30.449   | 151.451 | 616.08 | 33.634   |
| 50           | 168.525 | 768.15 | 30.449   | 151.451 | 673.88 | 33.634   |
| 51           | 168.525 | 768.15 | 30.449   | 151.451 | 751.16 | 33.634   |
| 52           | 54.387  | 601.68 | 30.449   | 25.01   | 511.11 | 33.634   |
| 72           | 6.0     | 489.65 | 45.801   | 4.024   | 516.79 | 47.80    |
| 73           | 6.0     | 492.27 | 59.421   | 4.024   | 518.49 | 57.966   |
| 74*          | 0.1733  | 330.15 | 59.421   | 0.1733  | 330.15 | 57.966   |
| 75           | 0.1733  | 330.15 | 59.421   | 0.1733  | 330.15 | 57.966   |

724 \* Stream with steam quality: 0.8988 in RC and 0.9398 in OS.

725

726 Finally, Table 9 compares the power generation in each steam turbine and the power  
 727 consumption in each pump obtained in both solutions. As can be seen, the net power generation in  
 728 both solutions is 63.026 MW, which is obtained in OS by producing 63.768 MW in the three steam  
 729 turbines (ST1, ST2, and ST3) since an amount of 0.742 MW is required to operate the pumps P8, P9,

730 and P10. While an amount of 64.001 MW is generated in RC, since the total consumption of the three  
 731 pumps (P1, P6, and P10) is 0.975 MW.

732

733 **Table 9.** Comparison of the electric power generated and required in RC and OS configurations.

| Turbine                | W [MW]                         |                |
|------------------------|--------------------------------|----------------|
|                        | RC (Franco and Giannini, 2006) | OS (This work) |
| HP steam turbine (ST1) | 8.307                          | 13.364         |
| MP steam turbine (ST2) | 24.329                         | 21.784         |
| LP steam turbine (ST3) | 31.365                         | 28.619         |
| Total                  | 64.001                         | 63.768         |
| Pump                   |                                |                |
| P1                     | 0.325                          | 0              |
| P2                     | 0                              | 0              |
| P3                     | 0                              | 0              |
| P4                     | 0                              | 0              |
| P5                     | 0                              | 0              |
| P6                     | 0.603                          | 0              |
| P7                     | 0                              | 0              |
| P8                     | 0                              | 0.689          |
| P9                     | 0                              | 0.048          |
| P10                    | 0.047                          | 0.005          |
| Total                  | 0.975                          | 0.742          |
| Net electric power     | 63.026                         | 63.026         |

734

735 Figure 11 illustrates the contribution of each steam turbine to the total power generation. In  
 736 both solutions, the largest fraction of the generated power is produced by the LP steam turbine (ST3)  
 737 and the lowest fraction by the HP steam turbine (ST1). Also, it can be seen that the HP steam turbine  
 738 generates more power in OS than in RC, contrary to what happens with the MP and LP steam turbines.

739 Table 10 summarizes the main differences between the RC and OS solutions.

740

741 **Table 10.** Main optimal (discrete and continuous) values associated with the synthesis and design of  
 742 the HRSG obtained in the RC and OS solutions.

|   | RC  | OS   |
|---|---|--|
| Total number of heat exchangers                         | 13  | 18   |
| Economizers   | 5   | 6  |
| Evaporators   | 3   | 3  |
| Superheaters  | 5   | 9  |
| Number of sections with parallel heat exchangers        | 4   | 6  |
| Number of inlet streams of the working fluid            | 1   | 3  |
| Number of pumps   | 3   | 3  |
| Location of the steam leaving turbine ST1 for reheating | After the first<br>superheater in<br>the MP level | After the<br>evaporator in<br>the MP level |
| Total flow rate of the working fluid (kg/s)             | 59.421  | 57.966                                     |

|  |        |        |
|--|--------|--------|
| Total heat recovered in HRSG (MW)  | 190.23 | 192.14 |
| Total heat transfer area required in HRSG ( $\times 10^3$ m <sup>2</sup> ) | 110290 | 94370  |
| Total power generated in steam turbines (MW)                               | 64.00  | 63.77  |
| Total power required by pumps (MW)   | 0.975  | 0.742  |

#### 743 5.4 Comparison of results considering an existing CCPP.

744 The proposed model was solved considering data reported in Almutairi et al. (2015)  
745 corresponding to a single block of the Sabiya CCPP, in Kuwait, which includes a 3P HRSG with 14  
746 heat exchangers arranged in series. Given the total electric power generated by the steam turbines –  
747 125.39 MW per HRSG i.e. 250.78 MW in total with two HRSGs – and the heat load – 351.69 MW  
748 required in each HRSG, the optimization problem consisted in finding the optimal HRSG  
749 configuration and operating conditions that minimize the total heat transfer area. The model is solved  
750 by allowing an economizer in each pressure level ( $EC_j=1$  in Eq.(22) for  $j=LP, MP, HP$ ), a superheater  
751 in the low pressure level and a superheater in the high pressure level ( $SH_j=1$  in Eq.(23) for  $j=LP,HP$ ),  
752 two superheaters in the medium pressure level ( $SH_j=2$  in Eq.(23) for  $j=MP$ ), and a maximum value of  
753 2 heat exchangers operating in parallel in each HRSG section ( $PE_i=2$  in Eq.(21)  $\forall i$ ).

754  
755 Figure 12 shows the obtained best configuration and the optimal operating conditions and sizes.  
756 Table 11 compares the number of heat exchangers involved in the Sabiya CCPP with that obtained in  
757 the optimal solution and the corresponding values of total heat transfer area required in each pressure  
758 level. Table 12 compares the contribution of each steam turbine to the desired electric power  
759 generation (125.39 MW). In Tables 11 and 12, the values of heat transfer area and electric power  
760 generated by each turbine of the Sabiya CCPP are calculated using the operating condition values  
761 reported in Almutairi et al. (2015) and the overall heat transfer coefficient values assumed in this  
762 study. In addition, the operating pressures in the three evaporators of the HRSG are the same as in  
763 Almutairi et al. (2015).

764 Regarding the HRSG configuration, Fig. 12 shows that the optimal solution requires 4 heat  
765 exchangers less than Almutairi et al. (2015) (10 vs. 14) and that the superheater in the LP level (6,LP)  
766 and the economizer in the HP level (6,HP) are arranged in parallel (section #6) while the remaining  
767 heat exchangers are arranged in series. The optimal configuration requires 245330 m<sup>2</sup> of heat transfer  
768 area, which represents by around 74% of that calculated for the Sabiya CCPP (331820 m<sup>2</sup>).

769 The total mass flowrate of the working fluid in the steam cycle obtained in the current solution  
770 is slightly higher than that required in the Sabiya CCPP solution (99.5 kg/s vs. 96.55 kg/s). The flow  
771 rates of the streams leaving the HP, MP, and LP levels (#51, #34, and #12) in the current solution are

40.4 kg/s, 95.1 kg/s, and 4.4 kg/s, respectively, while those in the Sabiya CCPP solution are 74.6 kg/s, 88.36 kg/s, and 8.97 kg/s, respectively.

**Table 11.** Comparison of the number of heat exchangers and heat transfer area between the obtained optimal solution with a solution corresponding to a single block of the Sabiya CCPP (125.39 MW).

|              | Number of HEXs                          |           | Total heat transfer area ( $\times 10^3 \text{ m}^2$ ) |           |
|--------------|---|-----------|--|-----------|
|              | Sabiya CCPP<br>(Almutairi et al., 2015) | This work | Sabiya CCPP<br>(Almutairi et al., 2015)                | This work |
| Economizers  | 5                                       | 3         | 189.25   | 113.49    |
| Evaporators  | 3                                       | 3         | 107.14   | 88.89     |
| Superheaters | 6                                       | 4         | 35.42  | 42.95     |
| Total        | 14                                      | 10        | 331.82   | 245.33    |

**Table 22.** Comparison of the electric power generated by steam turbines (125.39 MW per HRSG).

|                               | Sabiya CCPP<br>(Almutairi et al., 2015) | This work |
|-------------------------------|---|-----------|
| Total net electric power (MW) | 125.39                                  | 125.39    |
| HP turbine                    | 29.49                                   | 16.89     |
| IP turbine                    | 39.52                                   | 46.46     |
| LP turbine                    | 29.49                                   | 62.04     |

As shown in Table 12, the contribution of each steam turbine to the total electric power generation is different in both solutions. In the current solution, the largest contributor is the LP steam turbine with 62.04 MW, followed by the IP turbine with 46.46 MW. However, in the Sabiya CCPP solution, the largest contributor is the IP steam turbine with 39.52 MW, followed by the HP and LP steam turbines with 29.49 MW each.

Finally, it should be mentioned that the proposed approach of combining GDP with external routines for calculating the thermodynamic properties of fluids could be applied to other systems such as seawater desalination processes, cryogenic energy storage and air liquefaction, heat exchanger networks, water treatment processes, refrigeration processes. To this end, the first step is to develop a GDP model including the corresponding mass and energy balances as well as the sizing constraints. Then, the library containing the calculation of the thermodynamic properties of fluids is called from

794 GAMS by using *\$funclibin*. For other applications, it is possible to create new libraries (advanced  
795 user) or to use the wide variety of existing libraries (common user).

796 Beside the library *IAPWS.dll* employed in this work, the authors developed three general-  
797 purpose thermodynamic libraries that are available for their usage in the GAMS World Forum  
798 (<https://forum.gamsworld.org/viewtopic.php?t=11547&p=27414>). The former is called *RaoultLaw.dll*  
799 and is applicable for ideal solution. The second one is called *NRTLideal.dll* and includes the  
800 Nonrandom Two-Liquid (NRTL) activity coefficient model which is widely used in phase equilibrium  
801 calculations. And the third one is called *PengRobinson.dll* which includes the Peng Robinson equation  
802 of state. These libraries contain a database of 430 pure compounds.

## 804 6. Conclusions

805 A superstructure-based representation of three-pressure reheat combined-cycle power plants  
806 was conceived to derive a model of the process for simultaneous optimization of the configuration,  
807 design, and operation by applying generalized disjunctive programming and mixed-integer nonlinear  
808 programming formulations.

809 The optimization problem consisted in determining the way the heat exchangers and pumps of  
810 the heat recovery steam generator (HRSG) should be connected and the operating conditions and sizes  
811 of each process unit that minimize the total heat transfer area of the HRSG, while achieving a fixed,  
812 specified total net power generation level, given a flow rate and inlet temperature of the flue gas.

813 The superstructure model includes the possibility of selecting parallel, series, or combined  
814 parallel-series arrangements of heat exchangers in the hot, cold, and medium-temperature zones of the  
815 HRSG, as well as allowing the presence of more than one economizer and superheater at each pressure  
816 level. The inlet of the working fluid to the HRSG coming from the steam turbines for reheating can be  
817 located in the low-pressure level only, or in the low- and medium-pressure levels, or in all three  
818 pressure levels.

819 A model solution strategy based on a local search optimization algorithm based on the  
820 generalized reduced gradient was implemented in the General Algebraic Modeling System platform  
821 (GAMS). Extrinsic functions executed outside GAMS from dynamic-link libraries (DLL) – coded in  
822 the C programming language – were used to estimate the thermodynamic properties of the working  
823 fluids (flue gas and water/steam).

824 As a main result, improved process configurations of triple-pressure reheat HRSGs were  
825 obtained compared with respect to the reference cases reported in the literature.



826 The optimal solution obtained from the proposed superstructure was compared with a first  
827 reference case reported in the literature. Although the total heat loads in the HRSG in both studies are  
828 very similar (190.23 MW in the reference case and 192.14 MW in this work), the total heat transfer  
829 area required in this work is around 15% lower than the required in the reference case ( $91.74 \text{ m}^2$  vs.  
830  $107.70 \text{ m}^2$ ). This is due to the inclusion of 4 heat exchangers more than the reference case, making it  
831 possible to modify the configuration, include parallel exchanges along the HRSG, and obtain more  
832 appropriate driving forces in each heat exchanger. In both cases, the largest fraction of the generated  
833 power is produced by the low-pressure steam turbine and the smallest fraction by the high-pressure  
834 steam turbine.

835 Also, the optimal solution obtained from the proposed superstructure was compared with a  
836 second reference case corresponding to a single block of the existing Sabiya CCPP, located in Kuwait.  
837 For a same electric power generation (125.39 MW) and a total heat load in the HRSG (351.69 MW),  
838 the obtained optimal solution included 4 heat exchangers less (10 vs. 14) with a heat transfer area in  
839 the HRSG 26% less ( $245330 \text{ m}^2$  vs.  $331820 \text{ m}^2$ ).

840 This paper contributes to the literature with a solution strategy and a GDP mathematical  
841 optimization model of natural gas combined-cycle power plants operated at three pressure levels and  
842 the corresponding solution strategy, and with novel configurations of HRSG.

843 The proposed model relies on the calculation of several properties of streams through  
844 thermodynamic models that have several parameters subject to uncertainties. Additionally, the overall  
845 heat-transfer coefficients are subject to uncertainties. The discussed optimal designs may vary with  
846 these uncertainties. Therefore, sensitivity and uncertainty analysis are required to identify when and  
847 which parameters play a significant role in the error propagation. To this end, random sampling  
848 techniques such as Monte Carlo (MC) will be considered in future works.

849

#### 850 **Author statement**

851 **Juan I. Manassaldi:** Modeling, Methodology, Software, Visualization.

852 **Miguel C. Mussati:** Conceptualization, Discussion of Results, Writing - original draft.

853 **Nicolas J. Scenna:** Conceptualization, Discussion of Results, Draft review.

854 **Sergio F. Mussati:** Conceptualization, Discussion of Results, Writing - review & edition, Supervision.

855

856

857

858 Declaration of competing interests

859 None.

## 860 Acknowledgments

861 The Consejo Nacional de Investigaciones Científicas y Técnicas (CONICET) and the  
862 Universidad Tecnológica Nacional-Facultad Regional Rosario (UTN-FRRo) from Argentina are  
863 gratefully acknowledged for their financial support.

## 865 References

866 Ahadi-Oskui, T., Vigerske, S., Nowak, I., Tsatsaronis, G., 2010. Optimizing the design of complex  
867 energy conversion systems by Branch and Cut. *Computers & Chemical Engineering* 34 (8): 1226-1236.  
868 <https://doi.org/10.1016/j.compchemeng.2010.03.007>

869 Ahmadi, P., Dincer, I., 2011. Thermodynamic analysis and thermoeconomic optimization of a dual  
870 pressure combined cycle power plant with a supplementary firing unit. *Energy Convers Manage* 52(5), 2296–  
871 2308. <https://doi.org/10.1016/j.enconman.2010.12.023>

872 Ahmadi, P., Rosen, M.A., Dincer, I., 2012. Multi-objective exergy-based optimization of a  
873 polygeneration energy system using an evolutionary algorithm. *Energy* 46(1), 21–31.  
874 <https://doi.org/10.1016/j.energy.2012.02.005>

875 Ahmetovic, E., Grossmann, I.E., 2011. Global superstructure optimization for the design of integrated  
876 process water networks. *AIChE J* 57, 434–457. <https://doi.org/10.1002/aic.12276>

877 Almutairi, A., Pilidis, P., Al-Mutawa, N., 2015. Energetic and Exergetic Analysis of Combined Cycle  
878 Power Plant: Part-1 Operation and Performance. *Energies* 8, 14118–14135; doi:10.3390/en81212418

879 Ameri, M., Mokhtari, H., Sani, M.M., 2018. 4E analyses and multi-objective optimization of different  
880 fuels application for a large combined cycle power plant. *Energy* 156, 371–386.  
881 <https://doi.org/10.1016/j.energy.2018.05.039>

882 Bakhshmand, S.K., Saray, R.K., Bahlouli, K., Eftekhari, H., Ebrahimi, A., 2015. Exergoeconomic  
883 analysis and optimization of a triple-pressure combined cycle plant using evolutionary algorithm. *Energy* 93,  
884 555–567. <https://doi.org/10.1016/j.energy.2015.09.073>

885 Blumberg, T., Assar, M., Morozjuk, T., Tsatsaronis, G., 2017. Comparative exergoeconomic evaluation  
886 of the latest generation of combined-cycle power plants. *Energy Convers Manage*, 153, 616–626.  
887 <https://doi.org/10.1016/j.enconman.2017.10.036>

888 Bongartz, D., Najman, J., Mitsos, A., 2020. Deterministic global optimization of steam cycles using the  
889 IAPWS IF97 model. *Optimization and Engineering* 21, 1095-1131. <https://doi.org/10.1007/s11081-020-09502-1>

890 Boyaghchi, F., Molaie, H., 2015. Advanced exergy and environmental analyses and multi objective  
891 optimization of a real combined cycle power plant with supplementary firing using evolutionary algorithm.  
892 *Energy* 93, 2267–2279. <https://doi.org/10.1016/j.energy.2015.10.094>

- 893 Bracco, S., Siri, S., 2010. Exergetic optimization of single level combined gas–steam power plants  
894 considering different objective functions. *Energy* 35(12), 5365–5373.  
895 <https://doi.org/10.1016/j.energy.2010.07.021>
- 896 Brooke, A., Kendrick, D., Meeraus, A., 1992, GAMS: A User's Guide, Release 2.25. The Scientific  
897 Press, South San Francisco (CA).
- 898 Bruno, J.C., Fernandez, F., Castells, F., Grossmann, I.E., 1998. A rigorous MINLP model for the  
899 optimal synthesis and operation of utility plants. *Chem Eng Res Des* 76, 246–258.  
900 <https://doi.org/10.1205/026387698524901>
- 901 Bussieck, M., Drud, A., 2001. SBB: A New Solver for Mixed Integer Nonlinear Programming.  
902 [http://ftp.gamsworld.org/presentations/present\\_sbb.pdf](http://ftp.gamsworld.org/presentations/present_sbb.pdf)
- 903 Chen, J.J.J., 1987. Comments on improvements on a replacement for the logarithmic mean. *Chem Eng*  
904 *Sci* 42 (10), 2488–2489. [http://dx.doi.org/10.1016/0009-2509\(87\)80128-8](http://dx.doi.org/10.1016/0009-2509(87)80128-8).
- 905 Chen, Q., Grossmann, I., 2019. Modern Modeling Paradigms Using Generalized Disjunctive  
906 Programming. *Processes* 7(11), 839. <https://doi.org/10.3390/pr7110839>
- 907 Drud A., 1992. CONOPT A Large-Scale GRG Code. *Orsa Journal on Computing*, 6, 207–216.  
908 [https://www.gams.com/latest/docs/S\\_CONOPT.html](https://www.gams.com/latest/docs/S_CONOPT.html)
- 909 Elsidio, C., Mian, A., Martelli, E., 2017. MINLP A systematic methodology for the techno-economic  
910 optimization of Organic Rankine Cycles. *Energy Procedia* 129, 26–33.  
911 <https://doi.org/10.1016/j.egypro.2017.09.171>
- 912 Faria, D.C., Bagajewicz, M.J., 2012. A new approach for global optimization of a class of MINLP  
913 problems with applications to water management and pooling problems. *AIChE J* 58, 2320–2335.  
914 <https://doi.org/10.1002/aic.12754>
- 915 Franco, A., Giannini, N., 2006. A general method for the optimum design of heat recovery steam  
916 generators. *Energy* 31, 3342–3361. <https://doi.org/10.1016/j.energy.2006.03.005>
- 917 Franco, A., Russo A., 2002. Combined cycle plant efficiency increase based on the optimization of the  
918 heat recovery steam generator operating parameters. *Int J Therm Sci* 41 (9), 843–859.  
919 [https://doi.org/10.1016/S1290-0729\(02\)01378-9](https://doi.org/10.1016/S1290-0729(02)01378-9).
- 920 Gopalakrishnan, H., Kosanovic, D., 2015. Operational planning of combined heat and power plants  
921 through genetic algorithms for mixed 0–1 nonlinear programming. *Comp Oper Res* 56, 51–67.  
922 <https://doi.org/10.1016/j.cor.2014.11.001>
- 923 Grossmann, I., Lee, S., 2003. Generalized convex disjunctive programming: Nonlinear convex hull  
924 relaxation. *Computational Optimization and Applications* 26, 83–100. <https://doi.org/10.1023/A:1025154322278>
- 925 Grossmann, I., Ruiz, J., 2012. Generalized Disjunctive Programming: A Framework for Formulation  
926 and Alternative Algorithms for MINLP Optimization. *The IMA Volumes in Mathematics and its Applications*  
927 154, 93–115. [https://doi.org/10.1007/978-1-4614-1927-3\\_4](https://doi.org/10.1007/978-1-4614-1927-3_4)

- 928 IAPWS R7-97, 2012. The International Association for the Properties of Water and Steam Lucerne,  
929 Switzerland August 2007 . <http://www.iapws.org/relguide/IF97-Rev.pdf>
- 930 Izyan, Z.N., Noryani, M., Dayanasari, A.H., Shuhaimi, M., 2014. MINLP model for simultaneous  
931 scheduling and retrofit of refinery preheat train. *Inter J Energy and Environ* 5 (2), 197-206.
- 932 Jing, R., Wang, M., Wang, W., Brandon, N., Li, N., Chen, J., Zhao, Y., 2017. Economic and  
933 environmental multi-optimal design and dispatch of solid oxide fuel cell based CCHP system. *Energy Convers*  
934 *Manage* 154, 365–379. <https://doi.org/10.1016/j.enconman.2017.11.035>
- 935 Kaviri, A.G., Jaafar, M.M.N., Lazim, T.M., 2012. Modeling and multi-objective exergy based  
936 optimization of a combined cycle power plant using a genetic algorithm. *Energy Convers Manage* 258, 94–103.  
937 <https://doi.org/10.1016/j.enconman.2012.01.002>
- 938 Kim, J.S., Edgar, T.F., 2014. Optimal scheduling of combined heat and power plants using mixed-  
939 integer nonlinear programming. *Energy* 77, 675–690. <https://doi.org/10.1016/j.energy.2014.09.062>
- 940 Lee, S., Grossmann, I.E., 2000. New algorithms for nonlinear generalized disjunctive programming.  
941 *Comp Chem Eng* 24 (9–10), 2125-2141. [https://doi.org/10.1016/S0098-1354\(00\)00581-0](https://doi.org/10.1016/S0098-1354(00)00581-0)
- 942 León, E., Martín, M., 2016. Optimal production of power in a combined cycle from manure based  
943 biogas. *Energy Conversion and Management* 114, 89-99. <https://doi.org/10.1016/j.enconman.2016.02.002>
- 944 Lu, B., Huang, S., Grossmann, I.E., 2017. Optimal Synthesis and Operation of Wastewater Treatment  
945 Process with Dynamic Influent. *Ind Eng Chem Res* 56 (30), 8663-8676.  
946 <https://doi.org/10.1021/acs.iecr.7b01805>
- 947 Manassaldi, J.I., Mussati, M.C., Scenna, N.J., Mussati, S.F., 2019. Development of extrinsic functions  
948 for optimal synthesis and design—Application to distillation-based separation processes. *Comp Chem Eng* 125,  
949 532–544. <https://doi.org/10.1016/j.compchemeng.2019.03.028>
- 950 Manassaldi, J.I., Arias, A.M., Scenna, N.J., Mussati, M.C., Mussati, S.F., 2016. A discrete and  
951 continuous mathematical model for the optimal synthesis and design of dual pressure heat recovery steam  
952 generators coupled to two steam turbines. *Energy* 103, 807–823. <https://doi.org/10.1016/j.energy.2016.02.129>
- 953 Manassaldi, J.I., Mores, P.L., Scenna, N.J., Mussati, S.F., 2014. Optimal Design and Operating  
954 Conditions of an Integrated Plant Using a Natural Gas Combined Cycle and Postcombustion CO<sub>2</sub> Capture. *Ind*  
955 *Eng Chem Res* 53, 17026–17042. <https://doi.org/10.1021/ie5004637>
- 956 Martelli, E., Elsidio, C., Mian, A., Maréchal, F., 2017. MINLP Model and two-stage Algorithm for the  
957 Simultaneous Synthesis of Heat Exchanger Networks, Utility Systems and Heat Recovery Cycles. *Comp Chem*  
958 *Eng* 106, 663–689. <https://doi.org/10.1016/j.compchemeng.2017.01.043>
- 959 Mehrgoo, M., Amidpour, M., 2017. Configurations and pressure levels optimization of heat recovery  
960 steam generator using the genetic algorithm method based on the constructal design. *Appl Therm Eng* 122, 601–  
961 617. <https://doi.org/10.1016/j.applthermaleng.2017.04.144>
- 962 Mehrpanahi, A., Naserabad, S.N., Ahmadi, G., 2019. Multi-objective linear regression based  
963 optimization of full repowering a single pressure steam power plant. *Energy* 179, 1017–1035.

- 964 <https://doi.org/10.1016/j.energy.2019.04.208>
- 965 Mores, P.L., Manassaldi, J.I., Scenna, N.J., Caballero, J.A., Mussati, M.C., Mussati, S.F., 2018.
- 966 Optimization of the design, operating conditions, and coupling configuration of combined cycle power plants
- 967 and CO<sub>2</sub> capture processes by minimizing the mitigation cost. *Chem Eng J* 331, 870–894.
- 968 <https://doi.org/10.1016/j.cej.2017.08.111>
- 969 Morosuk, T., Tsatsaronis, G., 2011. Comparative evaluation of LNG e based cogeneration systems
- 970 using advanced exergetic analysis. *Energy* 36, 3771–3778. <http://dx.doi.org/10.1016/j.energy.2010.07.035>.
- 971 Mussati, S.F., Aguirre, P.A., Scenna, N.J., 2001. Optimal MSF plant design. *Desalination* 138, 341–347.
- 972 [https://doi.org/10.1016/S0011-9164\(01\)00283-1](https://doi.org/10.1016/S0011-9164(01)00283-1)
- 973 Mussati, S.F., Aguirre, P.A., Scenna, N.J., 2003. Novel configuration for a multistage flash-mixer
- 974 desalination system. *Ind Eng Chem Res* 42, 4828–4839. <https://doi.org/10.1021/ie020318v>
- 975 Mussati, S.F., Aguirre, P.A., Scenna, N.J., 2005. Optimization of alternative structures of integrated
- 976 power and desalination plant. *Desalination* 2005; 182: 123–129. <https://doi.org/10.1016/j.desal.2005.03.012>
- 977 Mussati, S.F., Aguirre, P.A., Scenna, N.J., 2003. Dual-purpose desalination plants. Part II. Optimal
- 978 configuration. *Desalination* 153, 185–189. [https://doi.org/10.1016/S0011-9164\(02\)01126-8](https://doi.org/10.1016/S0011-9164(02)01126-8)
- 979 Nadir, M., Ghenaiet, A., 2015. Thermodynamic optimization of several (heat recovery steam generator)
- 980 HRSG configurations for a range of exhaust gas temperatures. *Energy* 86, 685–695.
- 981 <https://doi.org/10.1016/j.energy.2015.04.023>
- 982 Naserabad, N.S., Mehrpanahi, A., Ahmadi, G., 2018. Multi-objective optimization of HRSG
- 983 configurations on the steam power plant repowering specifications. *Energy* 159, 277–293.
- 984 <https://doi.org/10.1016/j.energy.2018.06.130>
- 985 Oliva, D.G., Francesconi, J.A., Mussati, M.C., Aguirre, P.A., 2011. Modeling, synthesis and
- 986 optimization of heat exchanger networks. Application to fuel processing systems for PEM fuel cells. *Int J*
- 987 *Hydrogen Energy* 36 (15), 9098–9114. <https://doi.org/10.1016/j.ijhydene.2011.04.097>
- 988 Pérez-Uresti, S.I., Martín, M., Jiménez-Gutiérrez, A., 2019. Superstructure approach for the design of
- 989 renewable-based utility plants. *Comp Chem Eng* 123, 371–388.
- 990 <https://doi.org/10.1016/j.compchemeng.2019.01.019>
- 991 Rezaie, A., Tsatsaronis, G., Hellwig, U., 2019. Thermal design and optimization of a heat recovery
- 992 steam generator in a combined-cycle power plant by applying a genetic algorithm. *Energy* 168, 346–357.
- 993 <https://doi.org/10.1016/j.energy.2018.11.047>
- 994 Sahoo, P.K., 2008. Exergoeconomic analysis and optimization of a cogeneration system using
- 995 evolutionary programming. *Appl Therm Eng* 28, 1580–1588.
- 996 <https://doi.org/10.1016/j.applthermaleng.2007.10.011>
- 997 Santos, M.I., Uturbey, W., 2018. A practical model for energy dispatch in cogeneration plants. *Energy*
- 998 151, 144–159. <https://doi.org/10.1016/j.energy.2018.03.057>

999 Sahinidis, N.V., 2000. BARON Branch And Reduce Optimization Navigator.  
 1000 [https://www.gams.com/latest/docs/S\\_BARON.html](https://www.gams.com/latest/docs/S_BARON.html)

1001 Taccari, L., Amaldi, E., Martelli, E., Bisch, A., 2015. Short-Term Planning of Cogeneration Power  
 1002 Plants: a Comparison Between MINLP and Piecewise-Linear MILP Formulations. *Computer Aided Chemical*  
 1003 *Engineering* 37, 2429–2434. <https://doi.org/10.1016/B978-0-444-63576-1.50099-6>

1004 Tanvir, M.S., Mujtaba, I.M., 2008. Optimisation of design and operation of MSF desalination process  
 1005 using MINLP technique in gPROMS. *Desalination* 222, 419–430. <https://doi.org/10.1016/j.desal.2007.02.068>

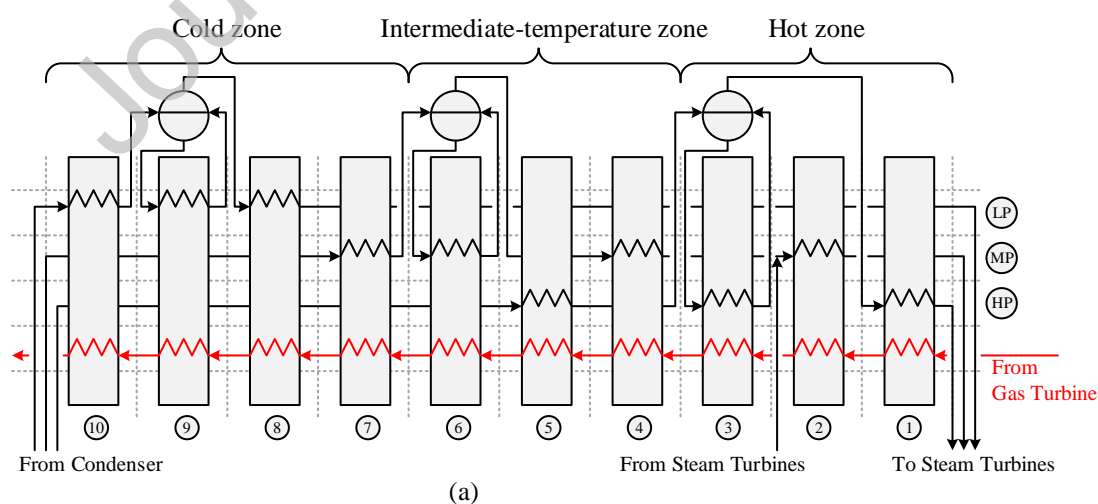
1006 Tsatsaronis, G., Park, M.H., 2002. On avoidable and unavoidable exergy destructions and investment  
 1007 costs in thermal systems. *Energy Convers Manage*, 43, 1259–1270.  
 1008 [http://dx.doi.org/10.1016/S0196-8904\(02\)00012-2](http://dx.doi.org/10.1016/S0196-8904(02)00012-2).

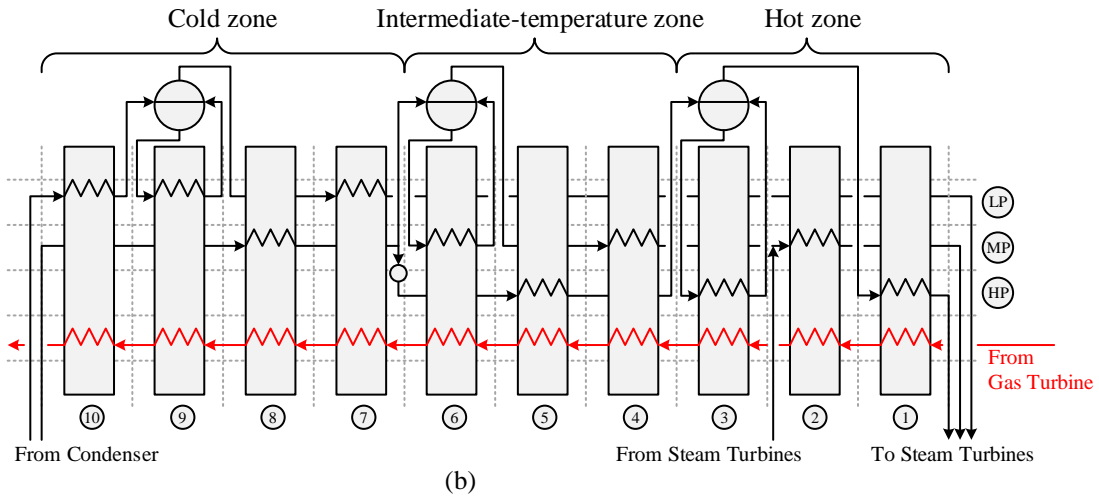
1009 Tsatsaronis, G., 1999. Strengths and limitations of exergy analysis. *Thermodynamic Optimization of*  
 1010 *Complex Energy Systems*. NATO Science Series (Series 3. High Technology), 69, 93–100.  
 1011 [https://doi.org/10.1007/978-94-011-4685-2\\_6](https://doi.org/10.1007/978-94-011-4685-2_6)

1012 Vecchietti, A., Lee, S., Grossmann, I.E., 2003. Modeling of discrete/continuous optimization problems:  
 1013 characterization and formulation of disjunctions and their relaxations. *Comp Chem Eng* 27 (3), 433–448.  
 1014 [https://doi.org/10.1016/S0098-1354\(02\)00220-X](https://doi.org/10.1016/S0098-1354(02)00220-X)

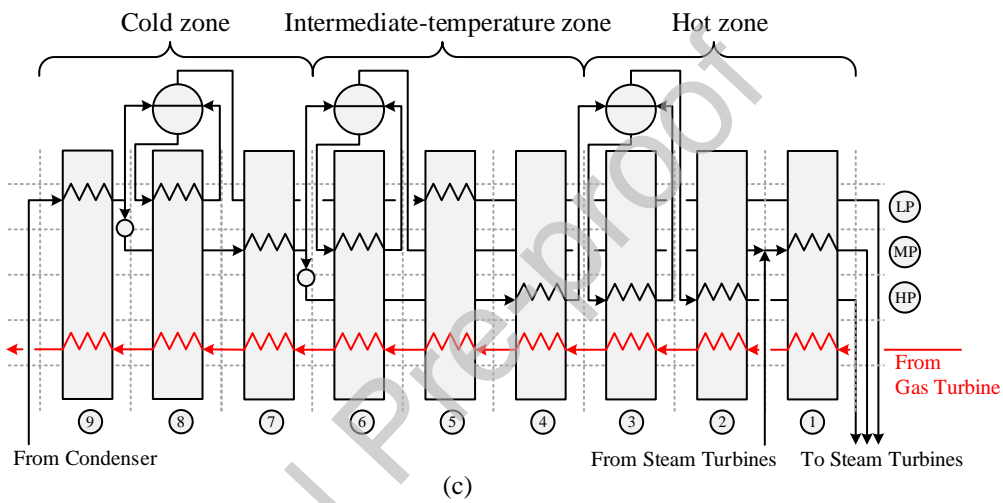
1015 Wang, L., Yang, Y., Dong, C., Morozuk, T., Tsatsaronis, G., 2014. Parametric optimization of  
 1016 supercritical coal-fired power plants by MINLP and differential evolution. *Energy Convers Manage* 85, 828–  
 1017 838. <https://doi.org/10.1016/j.enconman.2014.01.006>

1018 Zhang, J., Liu, P., Zhou, Z., Ma, L., Li, Z., Ni, W., 2014. A mixed-integer nonlinear programming  
 1019 approach to the optimal design of heat network in a polygeneration energy system. *Appl Energy* 114, 146–154.  
 1020 <http://dx.doi.org/10.1016/j.apenergy.2013.09.057>





(b)



(c)

**Figure 1.** Three candidate HRSG configurations differing in the way of feeding the working fluid at the different pressure levels and in the location of some heat exchangers: (a) simultaneous feeds in the three pressure levels, (b) simultaneous feeds in the low pressure (LP) and medium pressure (MP) levels, (c) feed in the LP level.

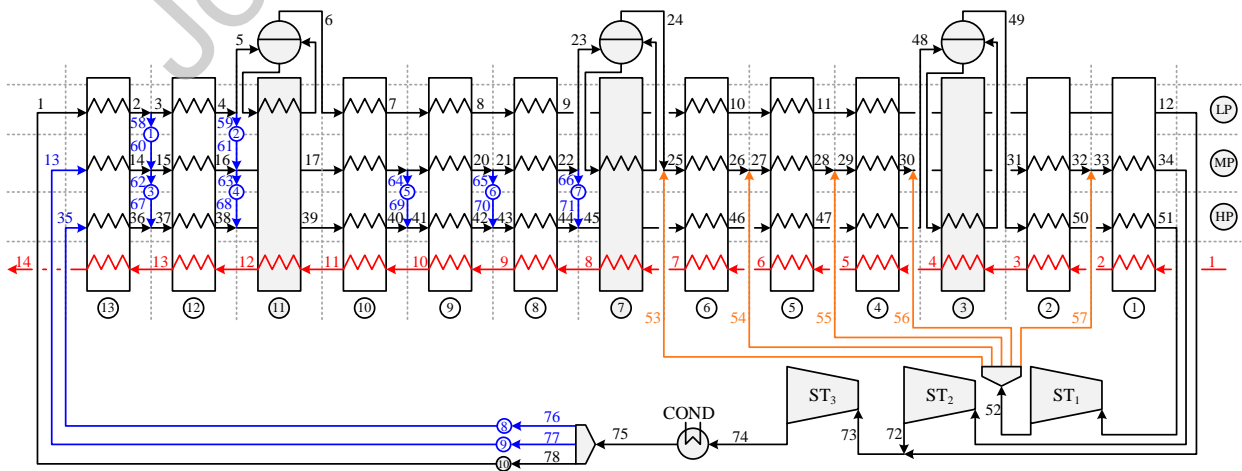


**Figure 2.** Process superstructure representation embedding many alternative HRSG configurations.

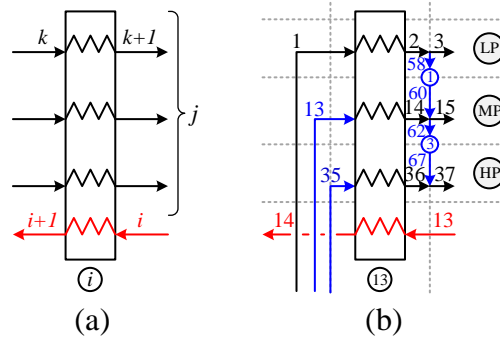


**Figure 3.** Representation and used nomenclature corresponding to a generic section ‘i’ (a) and to the section  $i=13$  as example (b).

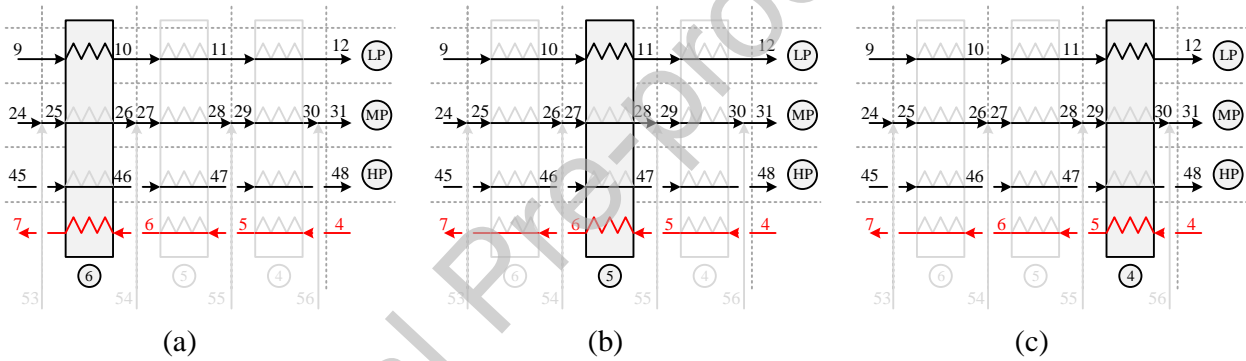


**Figure 4.** Equivalent solutions obtained when only one low-pressure (LP) superheater is selected in the sections  $i=4, 5,$  and  $6$ .

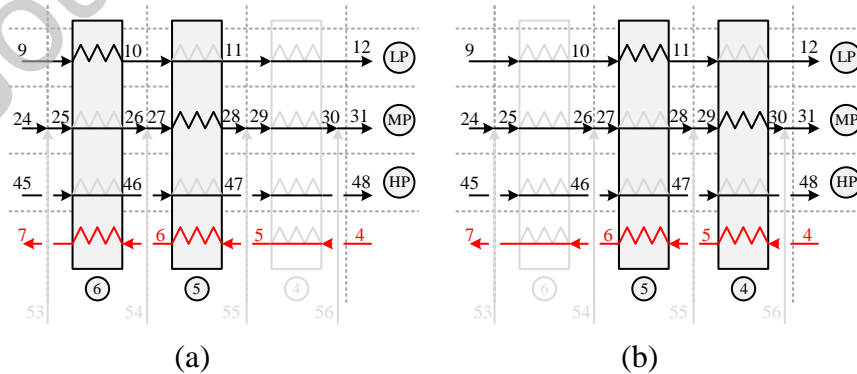


**Figure 5.** Equivalent solutions obtained when two heat exchangers are selected from the sections  $i=4, 5,$  and  $6$  and at the low-pressure (LP) and medium-pressure (MP) levels.



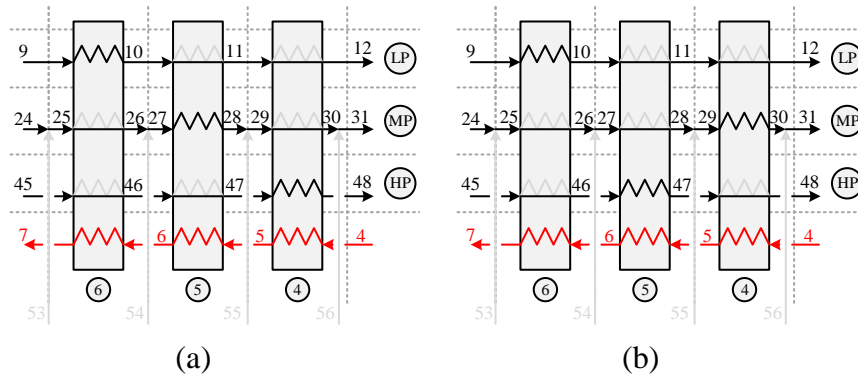


Figure 6. Different (no equivalent) solutions obtained when three heat exchangers are selected from the sections  $i=4, 5,$  and  $6$ .

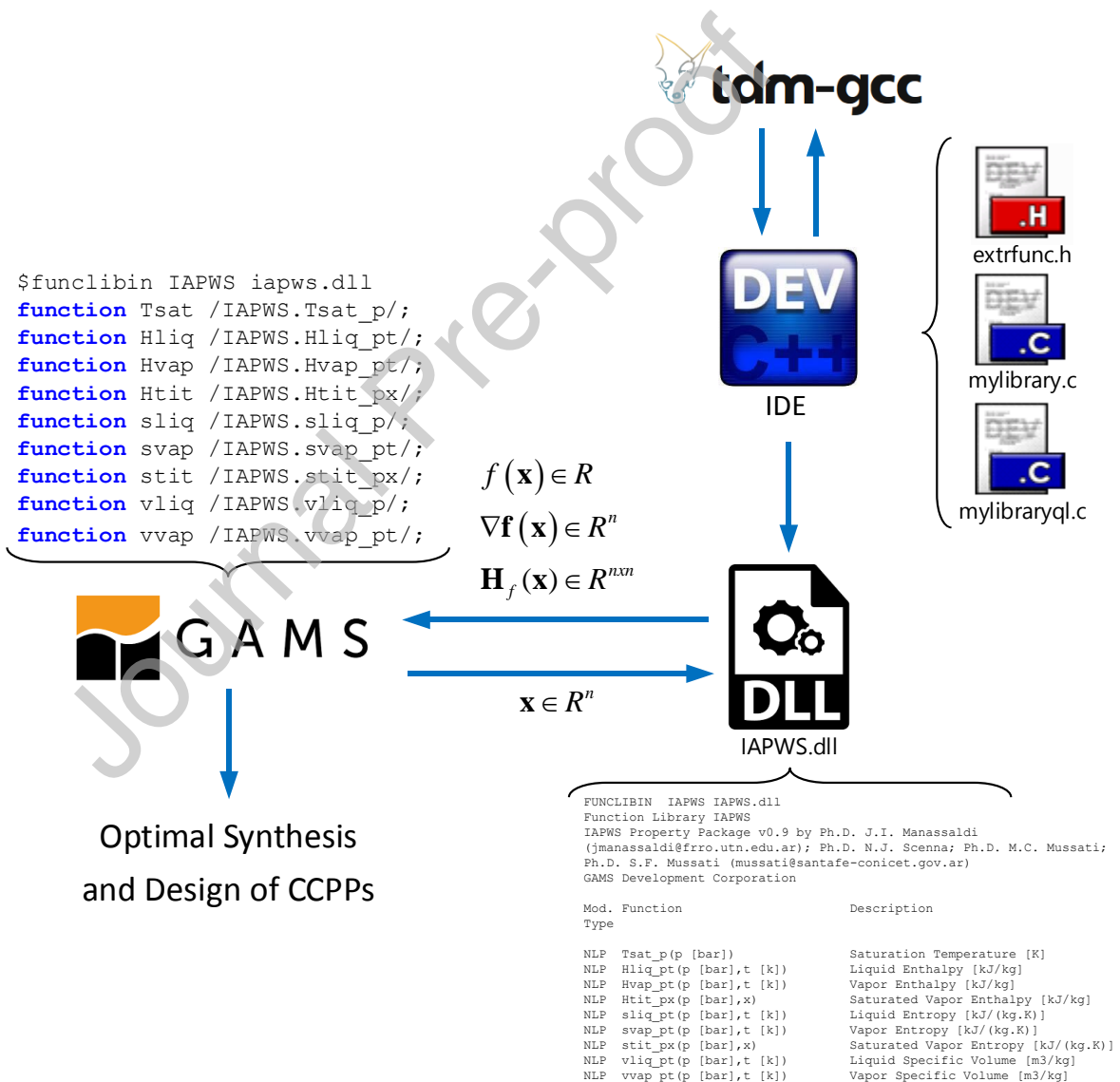
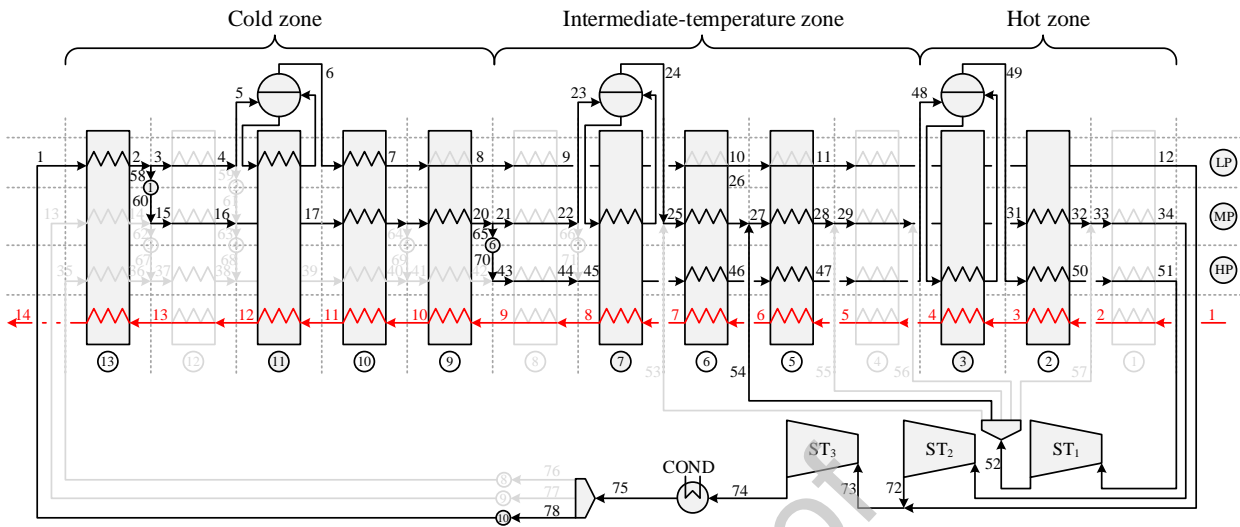


Figure 7. Main steps from the declaration to the execution of the extrinsic functions.

1052

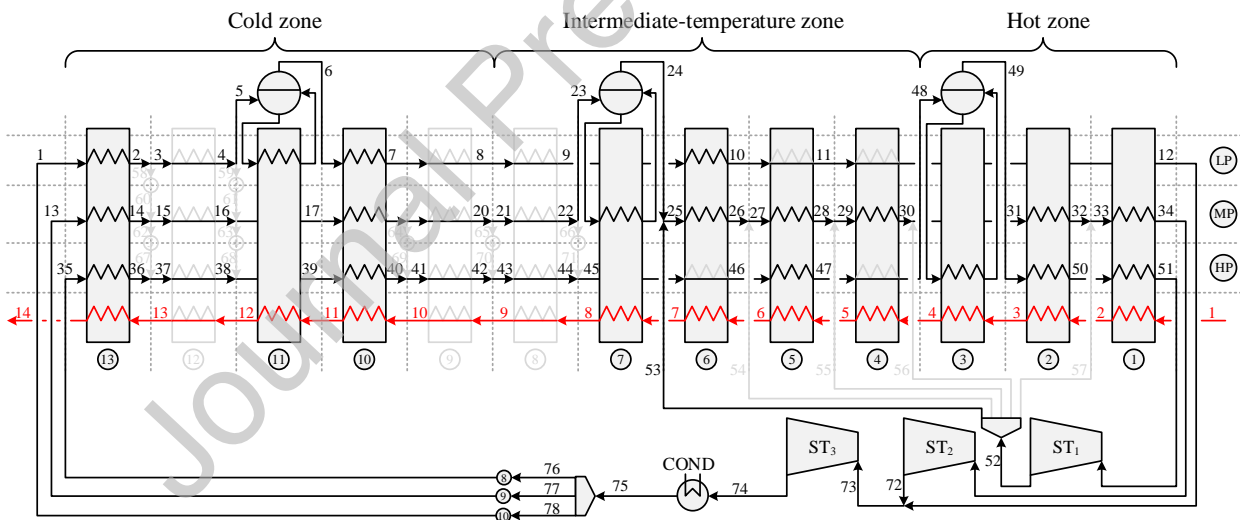


1053

1054

**Figure 8.** RC solution. Optimal configuration discussed in Franco and Giannini (2006).

1055

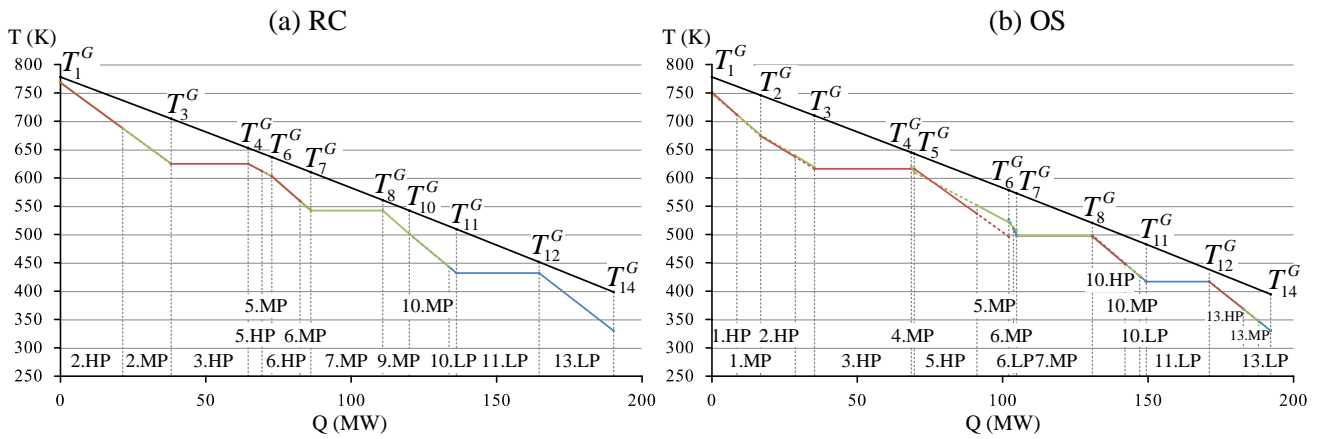


1056

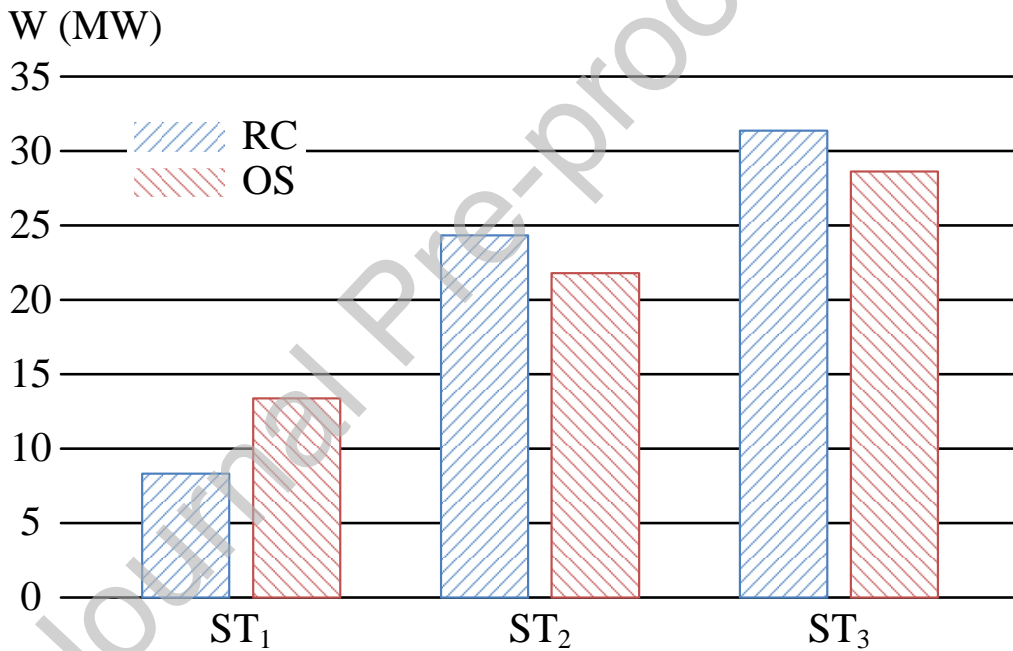
1057

1058

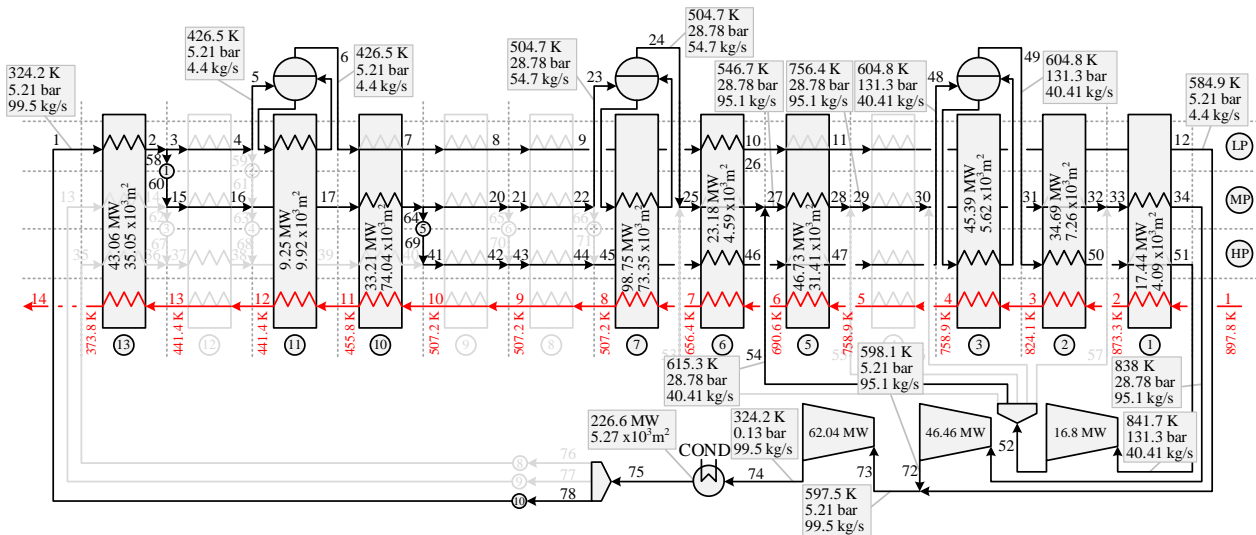
**Figure 9.** OS solution. Optimal configuration obtained considering the possibility of using parallel heat exchangers and repetition of economizers and superheaters at the same pressure level.



**Figure 10.** Temperature-enthalpy (T-H) diagram obtained for each configuration: (a) RC (Franco and Giannini, 2006), (b) OS (this work).



**Figure 11.** Comparison of the optimal electric power generated in each steam turbine in the configurations RC and OS.



1067  
 1068 . **Figure 12.** Optimal solution obtained for design specifications corresponding to the Sabiya  
 1069 combined-cycle power plant (Almutairi et al., 2015).